Journal of Infrastructure Intelligence and Resilience 3 (2024) 100082

Contents lists available at ScienceDirect

Journal of Infrastructure Intelligence and Resilience

journal homepage: www.journals.elsevier.com/journal-of-infrastructure-intelligence-and-resilience

Control of seismic induced response of wind turbines using KDamper

Haoran Zuo [a], Xunyi Pan [a], Kaiming Bi [b,*], Hong Hao [a,c,**]

[a] Centre for Infrastructural Monitoring and Protection, School of Civil and Mechanical Engineering, Curtin University, Kent Street, Bentley, WA 6102, Australia
[b] Department of Civil and Environmental Engineering, The Hong Kong Polytechnic University, Kowloon, Hong Kong, China
[c] Earthquake Engineering Research and Test Center, Guangzhou University, Guangzhou, China

ARTICLE INFO

Keywords:
Wind turbine
Structural vibration control
Seismic load
KDamper

ABSTRACT

Earthquake-induced vibrations of wind turbines may compromise structural serviceability and safety. Most previous studies adopted passive control devices to mitigate the seismic responses of wind turbines. However, their control effectiveness is heavily dependent on the mass ratio between control devices and wind turbines, and they were typically housed at the tower top or within the nacelle. The restricted space within the hollow tower and the nacelle imposes considerable challenges for the implementation of such devices, rendering the application of large-scale control devices unfeasible for structural vibration control of wind turbines. To this end, this paper integrates a negative stiffness element within a conventional tuned mass damper (TMD), termed KDamper, to mitigate vibrations of wind turbine towers under seismic loads. Specifically, the widely used NREL 5 MW wind turbine is selected as a prototype structure and its tower is modelled as a multiple-degree-of-freedom system. Then KDamper is incorporated into the developed model and its parameters are optimized based on the H_2 criterion. Subsequently, the control effectiveness of KDamper is investigated and compared with TMD in the frequency domain, and the control performances in terms of the effectiveness and robustness of KDamper are further examined under a series of earthquake records. Results show that KDamper has superior control effectiveness and robustness than TMD, indicating it has considerable potential for application in improving wind turbine performances against earthquake hazards.

1. Introduction

As a sustainable and clean energy source, wind power has attracted extensive attention in recent years, and the installation of wind turbines has increased rapidly. Nearly 78 GW of wind power capacity was added worldwide in 2022 (GWEC, 2022). With the wind industry expansion, wind turbines are increasingly being installed in earthquake-prone regions (Wang et al., 2021; Zhang et al., 2022). In addition, tall towers and long blades are designed and manufactured to harvest more wind resources, which makes wind turbine structures more vulnerable to external excitations.

A significant amount of research has been devoted to using various control devices to mitigate wind turbine vibrations, and these control devices can be divided into passive, semi-active, and active types (Rahman et al., 2015). Considering soil-monopile interaction and structural damage would change structural frequencies, Hemmati and Oterkus (2018), Leng et al. (2023), and Sun (2018) used a semi-active tuned mass damper (TMD) to reduce tower responses under wind, wave and seismic loads; Sarkar and Chakraborty (2018) used multiple semi-active magneto-rheological tuned liquid column dampers (TLCDs); Alkhoury et al. (2022), Brodersen et al. (2017), Fitzgerald et al. (2018), and Hu et al. (2017) used an active TMD to enhance the structural performances of wind turbines, to name a few. Compared to passive control, semi-active and active control achieve better effectiveness at the expense of external energy, however, they also inevitably increase the complexity of the control system and raise potential instability concerns. Conversely, passive control is straightforward without energy consumption and develops forces in response to the motions of the protected structure. The most widely used passive control device is TMD, and different TMD implementations in wind turbines have been proposed, such as a single TMD positioned at the top of the tower or within the nacelle (Bernuzzi et al., 2021; Ghassempour et al., 2019; Lin et al., 2021; Liu et al., 2020), a bi-directional TMD to simultaneously control tower responses in both fore-aft and side-to-side directions (Zhao et al., 2018; Zuo et al., 2020), multiple TMDs installed along the tower height to mitigate multiple modes (Chen et al., 2021; Hussan et al., 2018; Wang

* Corresponding author. Department of Civil and Environmental Engineering, The Hong Kong Polytechnic University, Kowloon, Hong Kong, China.
** Corresponding author. Earthquake Engineering Research and Test Center, Guangzhou University, Guangzhou, China.
E-mail addresses: kaiming.bi@polyu.edu.hk (K. Bi), hong.hao@curtin.edu.au (H. Hao).

https://doi.org/10.1016/j.iintel.2024.100082
Received 25 November 2023; Received in revised form 26 December 2023; Accepted 1 January 2024
Available online 3 January 2024

et al., 2020), and TMD variants (e.g., pendulum (Chapain and Aly, 2021; Colherinhas et al., 2022; Jahangiri et al., 2021; Liu et al., 2022b) and prestressed (Liu et al., 2021) TMDs), etc. Liquid has also been proposed to serve as an energy dissipator, such as TLCD (Ding et al., 2023) and tuned liquid damper (TLD) (Chen and Georgakis, 2013; Zhang et al., 2019b). Moreover, some researchers adopted dissipative elements only (e.g., viscous dampers (Dai et al., 2021; Wang et al., 2023)) to control tower vibrations. The aforementioned passive control devices have been proven effective in suppressing the responses of wind turbine towers, by either numerical simulations or experimental tests.

It is worth noting that the effectiveness of passive control devices is heavily dependent on an auxiliary mass, and an increment in the auxiliary mass improves the effectiveness. However, the narrow space in wind turbines limits the installation of a large control device. Moreover, in addition to the heavy rotor-nacelle assembly (accounting for approximately 50% of the whole system's weight) located at the tower top, a large auxiliary mass will increase the self-weight of wind turbines, which, in turn, may lead to the instability and violent vibrations of wind turbines. Furthermore, TMD is only effective in the target frequency (e.g., typically the frequency corresponding to the fundamental vibration mode) and it lacks control robustness. Given that seismic ground motions are non-stationary stochastic excitations with energy distributed in a broad frequency range, the control performances of TMD in mitigating earthquake-induced vibrations of wind turbines are not always desirable.

To address the above limitations of TMD, many improved methods were proposed. For example, (1) an inerter that can transfer the rotational motions into the linear motions to amplify the physical mass was incorporated into the conventional TMD (Ikago et al., 2012; Smith, 2002). Using inerter to alleviate the attached mass in the vibration control of wind turbines was investigated by Chen et al. (2023) and Zhang et al. (2019a, 2023), and it was concluded that better control effectiveness could be achieved by connecting the inerter to locations away from the tower top. (2) Nonlinear energy sinks (NESs) can resonate with structures at any frequency due to their inherent nonlinear characteristics. Zuo et al. (2022) and Zuo and Zhu (2022) designed track NESs to reduce wind turbine responses against wind, sea waves, and earthquakes, and comparable effectiveness but superior robustness to TMD were achieved.

Furthermore, the concept of negative stiffness element was proposed and applied in structural isolation by Molyneux (1957). The primary purpose of the negative stiffness element is to markedly reduce the stiffness of the protected structure, aiming to minimize the transmission of force or displacement, especially in cases involving a broader range of excitation frequencies. However, the application of only a negative stiffness element limits the static loading capacity of the protected structure due to the reduced stiffness. Combining negative stiffness elements with positive stiffness components in series or parallel lays a foundation for a series of innovative negative stiffness damper designs. Li et al. (2020) provided a comprehensive review of the recent research and developments on negative stiffness dampers. This strategic combination allows negative stiffness dampers to achieve a high level of isolation performance while maintaining the load-carrying capacity of structures in the static state (Li et al., 2020). Various mechanisms have been reported to realise the negative stiffness such as coil springs (Le and Ahn, 2011, 2012, 2013; Molyneux, 1957), disk springs (Niu et al., 2014), pre-bulked beams (Huang et al., 2014; Liu et al., 2013), and magnetism (Shi and Zhu, 2015; Xu et al., 2013), and the effectiveness of negative stiffness dampers in engineering structures was demonstrated (Attary et al., 2015; Pasala et al., 2013). Moreover, Liu and Ikago (2021b, 2022a, 2022b, 2022c), Liu and Liu (2023), and Liu et al. (2022a, 2023) have employed a configuration wherein a negative stiffness and a Maxwell element (consisting of spring and damping elements connected in series) are combined in parallel, referred to as a rate-independent damping device. This setup has been used as an isolator to control low-frequency structural vibrations. As previously noted, wind turbines feature tall towers and heavy rotors, and they vibrate at a low frequency. Hence, the rate-independent damping device could be another viable approach for mitigating wind turbine responses.

Based on the two-degree-of-freedom negative stiffness oscillator in (Antoniadis et al., 2015), Antoniadis et al. (2018) further proposed a negative stiffness damper dubbed KDamper. Fig. 1 shows schematics of TMD and KDamper, where m_S and k_S denote the mass and stiffness of the primary structure, respectively; m_D and c_D are the auxiliary mass and damping coefficient, respectively; k_P and k_N are the positive stiffness and negative stiffness, respectively. It should be noted that the inherent damping of the primary structure is ignored in Fig. 1. By introducing a negative stiffness element to the auxiliary mass, the amplitudes of the inertia force of the auxiliary mass and the negative stiffness force are totally in phase, and thus the inertia effect of the auxiliary mass is retained or even amplified without increasing the mass. The applications of KDamper in engineering structures were recently reported (Kampitsis et al., 2022; Kapasakalis et al., 2020, 2021; 2023; Sapountzakis et al., 2017). The results indicated that although the KDamper incorporates a negative stiffness element, it is designed to be statically and dynamically stable while, compared to conventional control devices, its control effectiveness is more significant.

The present study proposes using KDamper for seismic performance enhancement of wind turbines. Specifically, different connecting configurations and stiffness ratios between negative and positive stiffness are considered, and the control performances of KDamper are investigated and compared to the traditional TMD in both frequency and time domains. The paper is structured as follows: the numerical models of the wind turbines without and with control are developed in Section 2; the optimal design of KDamper and TMD is introduced in Section 3; the frequency domain analyses of the wind turbines without and with control are performed in Section 4; the control effectiveness and robustness of KDamper are systematically examined under a series of earthquake records and compared to TMD; the main conclusions are summarized in Section 6; some future research endeavours are addressed in Section 7.

2. Numerical model

2.1. Wind turbine properties

The horizontal-axis three-blade wind turbine reported by Jonkman et al. (2009) is chosen for seismic response analysis and control performance investigation in the present study. The selected wind turbine features a rated capacity of 5 MW with a rotor diameter of 126 m and a tower height of 87.6 m. Table 1 presents the gross properties of the NREL 5 MW wind turbine, and the thickness of the tower is increased by 30% to ensure that the first fore-aft and side-to-side tower frequencies are within one and three times rotational frequencies throughout the operational range of the wind turbine. The material density of the tower is 8500 kg/m^3 considering the connection parts (e.g., bolts, welds, and flanges) and paint in the tower, which is slightly larger than the standard steel density of 7850 kg/m^3. Moreover, the mass density, sectional flexural rigidity, and mass moment of inertia density along the height of the tower can be calculated based on the geometrical dimensions and material properties in Table 1, and the calculated results are given in Table 2.

2.2. Wind turbine without control

The efficacy of using KDamper to mitigate the tower responses induced by seismic loads is of interest, and the wind turbine is assumed in the parked condition in the present study. As a result, only the tower is modelled as a multiple-degree-of-freedom (MDOF) system, and the rotor-nacelle assembly (i.e., three blades, hub, and nacelle) is considered as a concentrated mass and a mass moment of inertia at the tower top. The discretization and the analytical model of the wind turbine are

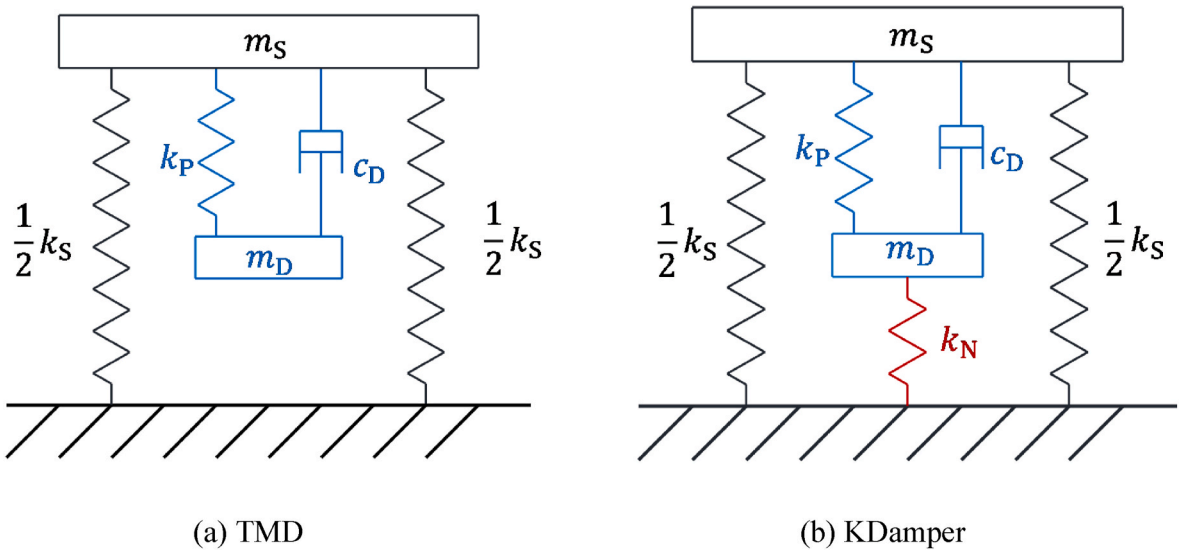

Fig. 1. Schematics of (a) TMD and (b) KDamper.

Table 1
Gross properties of the NREL 5 MW wind turbine.

Rotor diameter	126 m
Tower height	87.6 m
Diameters of the tower top and base	3.87 m and 6 m
Wall thickness at the tower top and base	0.019 m and 0.027 m
Rotor mass	110,000 kg
Nacelle mass	240,000 kg
Tower mass	347,460 kg
Material density of the tower	8500 kg/m^3
Young's modulus of the tower	210 GPa

shown in Fig. 2. Specifically, the tower is equally divided into 10 elements with an element length of 8.76 m. The translational ($x_n, n = 1, 2, \ldots 10$ in Fig. 2) and rotational (θ_n) degrees-of-freedom (DOFs) at each element node are considered, totalling 20 DOFs for the wind turbine without control. The mass matrix of the wind turbine without control is expressed as

$$\boldsymbol{M}_{\mathbf{wc}} = \begin{bmatrix} m_1 & & & & & \\ & J_1 & & & & \\ & & \ddots & & & \\ & & & m_{10}+m_{\mathrm{RNA}} & & \\ & & & & J_{10}+J_{\mathrm{RNA}} & \end{bmatrix}_{20\times 20} \tag{1}$$

where m_n and J_n $(n = 1, 2, \ldots, 10)$ are the mass and mass moment of inertia at an element node, and they can be obtained by the average of the density (Table 2) between two adjacent cross-sections times the element length of 8.76 m; m_{RNA} and J_{RNA} are the mass and mass moment of inertia of the rotor-nacelle assembly, respectively. The nth element stiffness matrix is given as follows:

$$\boldsymbol{k}_n = \begin{bmatrix} A_n & B_n \\ C_n & D_n \end{bmatrix}_{4\times 4} \tag{2}$$

where

$$A_n = \begin{bmatrix} \frac{12EI_n}{L^3} & \frac{6EI_n}{L^2} \\ \frac{6EI_n}{L^2} & \frac{4EI_n}{L} \end{bmatrix},\ B_n = \begin{bmatrix} -\frac{12EI_n}{L^3} & \frac{6EI_n}{L^2} \\ -\frac{6EI_n}{L^2} & \frac{2EI_n}{L} \end{bmatrix},\ C_n = \begin{bmatrix} -\frac{12EI_n}{L^3} & -\frac{6EI_n}{L^2} \\ \frac{6EI_n}{L^2} & \frac{2EI_n}{L} \end{bmatrix},\ D_n = \begin{bmatrix} \frac{12EI_n}{L^3} & -\frac{6EI_n}{L^2} \\ -\frac{6EI_n}{L^2} & \frac{4EI_n}{L} \end{bmatrix} \tag{3}$$

Similarly, the flexural rigidity of an arbitrary element (EI_n) is defined as the average of the sectional flexural rigidity (Table 2) between two adjacent cross-sections, and L is the element length. The stiffness matrix of the wind turbine without control is formed by assembling these element stiffness matrices as

$$\boldsymbol{K}_{\mathbf{wc}} = \begin{bmatrix} D_1+A_2 & B_2 & & & & \\ C_2 & D_2+A_3 & B_3 & & & \\ & C_3 & \ddots & \ddots & & \\ & & \ddots & D_9+A_{10} & B_{10} & \\ & & & C_{10} & D_{10} & \end{bmatrix}_{20\times 20} \tag{4}$$

Table 2
Distributed tower properties.

Elevation (m)	Height fraction	Mass density (kg/m)	Sectional flexural rigidity (N·m^2)	Inertia density (kg·m)
0.00	0.0	5590.87	614.34E+9	2,4865.3
8.76	0.1	5232.42	534.82E+9	2,1646.7
17.52	0.2	4885.76	463.27E+9	1,8750.6
26.28	0.3	4550.87	399.13E+9	1,6154.7
35.04	0.4	4227.75	341.88E+9	1,3837.6
43.80	0.5	3916.40	291.01E+9	1,1778.6
52.56	0.6	3616.83	246.03E+9	9957.8
61.32	0.7	3329.03	206.46E+9	8356.3
70.08	0.8	3053.01	171.85E+9	6955.6
78.84	0.9	2788.75	141.78E+9	5738.3
87.60	1.0	2536.27	115.82E+9	4687.7

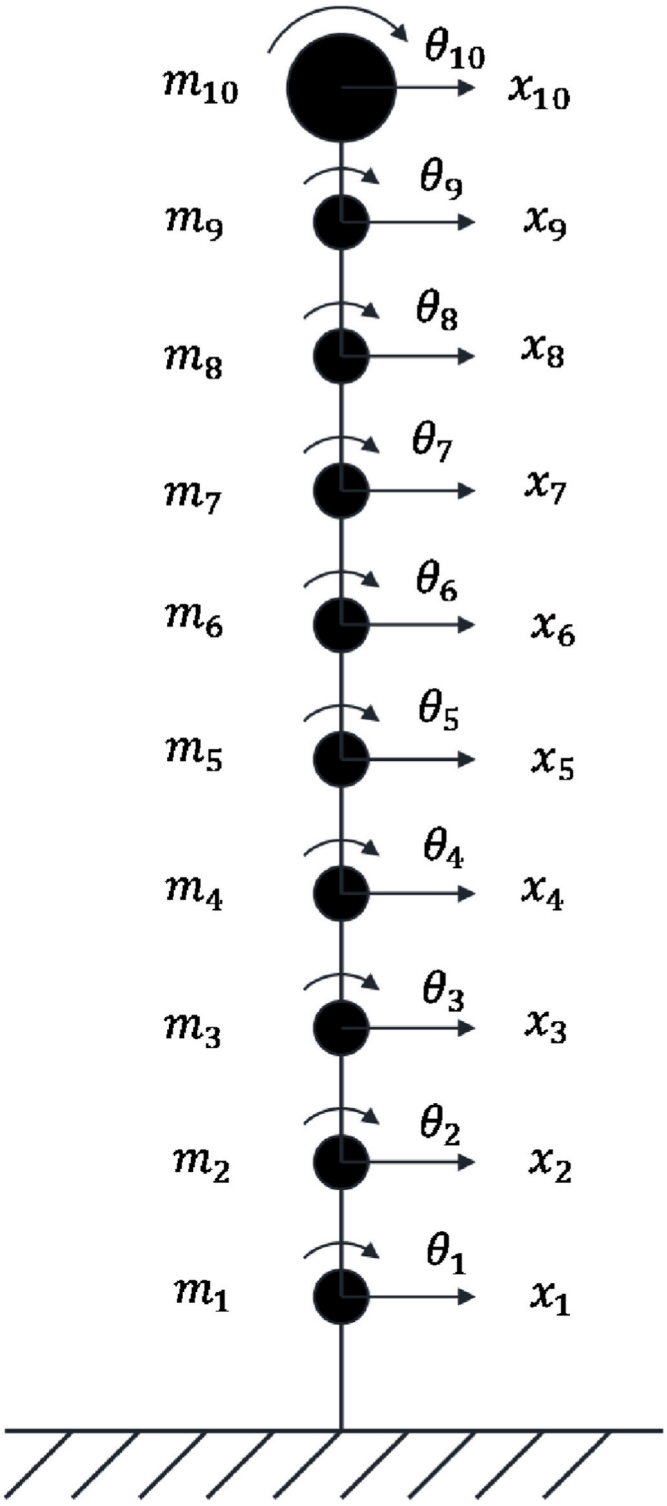

Fig. 2. Discretization and analytical model of the wind turbine.

Table 3
Natural frequencies of the wind turbine.

Mode	Present study	Study by Jonkman et al. (2009)
First	0.3357 Hz	0.3240 Hz
Second	3.0585 Hz	2.9003 Hz

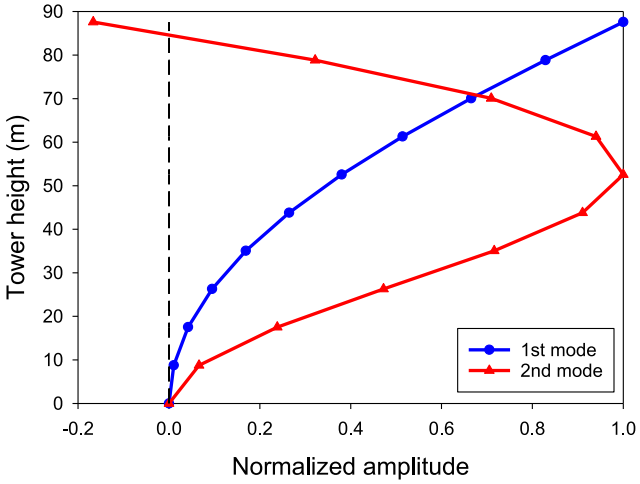

Fig. 3. First two mode shapes of the tower.

Subsequently, an eigenvalue analysis is performed to calculate the natural frequencies and mode shapes of the tower by using the developed mass and stiffness matrices. Table 3 tabulates the natural frequencies corresponding to the first and second vibration modes and Fig. 3 shows the mode shapes. As shown, the frequencies of the tower obtained in the present study agree well with those given by Jonkman et al. (2009). In addition, a damping ratio of 2% is assumed for the first two vibration modes and the damping matrix of the wind turbine without control is thus developed by using Rayleigh damping (i.e., $\boldsymbol{C}_{\mathrm{wc}} = \alpha \boldsymbol{M}_{\mathrm{wc}} + \beta \boldsymbol{K}_{\mathrm{wc}}$, in which α and β are the mass and stiffness coefficients).

2.3. Wind turbine with control

The control performances of KDamper in reducing earthquake-induced responses of the wind turbine are also compared to the traditional TMD in the present study, and Fig. 4 shows the connecting configurations of KDamper and TMD within the wind turbine. As shown, the auxiliary mass (m_{D}) in KDamper or TMD is connected to the top mass point (m_{10}) using a positive stiffness spring element (k_{P}) and a dashpot element (c_{D}). Moreover, to find out the optimal configuration of KDamper, the additional mass is also connected to the mass points below the tower top (i.e., $m_9, m_8, \ldots, m_1$) and the ground, respectively, using a negative stiffness spring element (k_{N}). It is worth noting that, in the following analysis, external excitations are assumed to act exclusively in the fore-aft direction of the tower (x direction in Fig. 4). This assumption allows for a more focused examination of the tower's responses to excitations in the primary direction of interest while providing valuable insights into the system's dynamic behaviour and the performances of the control devices.

Fig. 5 illustrates a conceptual design of KDamper installed in the wind turbine tower. As shown, the positive stiffness and damping in KDamper are analogous to a pendulum TMD (Soltani and Deraemaeker, 2022), and the auxiliary mass is supported by two oblique springs, which are connected to an arbitrary location of the tower. When the auxiliary mass moves with a displacement of x, the resultant force (F) generated by these two springs in the fore-aft direction is

$$F = 2k_1 \left(\frac{\sqrt{l_1^2 + l_2^2}}{\sqrt{l_1^2 + (l_2 - x)^2}} - 1 \right) (l_2 - x) \tag{5}$$

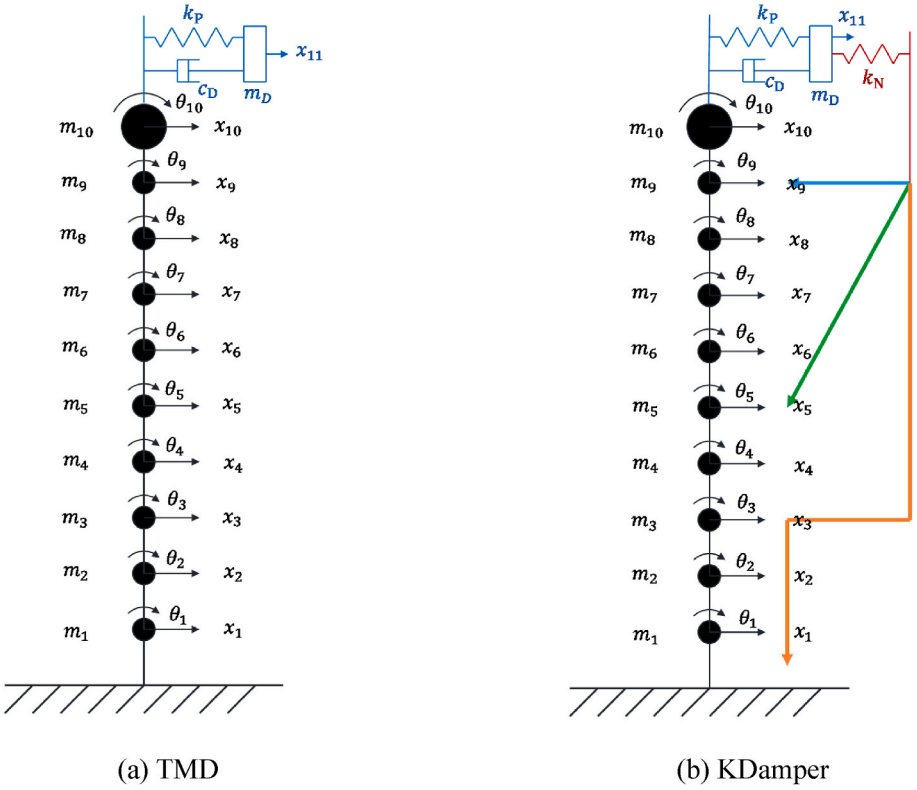

Fig. 4. Connecting configurations between control devices and wind turbine.

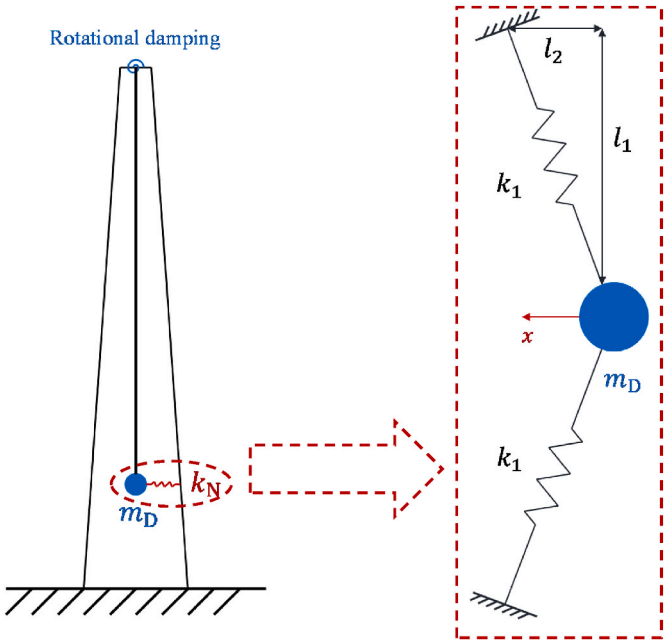

Fig. 5. Conceptual design of KDamper in the wind turbine tower.

where k_1 is the stiffness of the oblique springs; l_1 and l_2 are the vertical and horizontal lengths of the oblique springs, respectively. The resultant stiffness of these two springs can be obtained by differentiating Eq. (5) to x as

$$k = -2k_1\frac{\sqrt{l_1^2+l_2^2}}{\sqrt{l_1^2+(l_2-x)^2}} + 2k_1(l_2-x)^2\frac{\sqrt{l_1^2+l_2^2}}{\left[l_1^2+(l_2-x)^2\right]^{3/2}} \tag{6}$$

As indicated in Eq. (6), a negative stiffness is generated. The mass, stiffness, and damping matrices of the wind turbine without control have been developed in Section 2.2, however, these matrices should be changed accordingly after the implementation of KDamper and TMD. In addition, the wind turbine with TMD can be deemed a special case of KDamper by setting the negative stiffness as zero. Therefore, only the mass, damping, and stiffness matrices of the wind turbine with KDamper are introduced as follows:

The mass and damping matrices of the wind turbine with KDamper are given by

$$\boldsymbol{M}_{\mathbf{c}} = \begin{bmatrix} \boldsymbol{M}_{\mathbf{wc}} & [0]_{20\times 1} \\ [0]_{1\times 20} & m_{\mathrm{D}} \end{bmatrix}_{21\times 21} \tag{7}$$

$$\boldsymbol{C}_{\mathbf{c}} = \begin{bmatrix} \boldsymbol{C}_{\mathbf{wc}} & [0]_{20\times 1} \\ [0]_{1\times 20} & 0 \end{bmatrix}_{21\times 21} + \begin{bmatrix} [0]_{18\times 18} & [0]_{18\times 3} \\ [0]_{3\times 18} & c_1 \end{bmatrix}_{21\times 21} \tag{8}$$

where c_1 has the following form

$$c_1 = \begin{bmatrix} c_{\mathrm{D}} & 0 & -c_{\mathrm{D}} \\ 0 & 0 & 0 \\ -c_{\mathrm{D}} & 0 & c_{\mathrm{D}} \end{bmatrix}_{3\times 3} \tag{9}$$

When the negative stiffness element is connected to the nth mass point ($n = 1, 2, \ldots, 9$), the stiffness matrix of the wind turbine with KDamper is

$$\boldsymbol{K}_{\mathbf{c}} = \begin{bmatrix} \boldsymbol{K}_{\mathbf{wc}} & [0]_{20\times 1} \\ [0]_{1\times 20} & 0 \end{bmatrix}_{21\times 21} + \begin{bmatrix} [0]_{18\times 18} & [0]_{18\times 3} \\ [0]_{3\times 18} & k_1 \end{bmatrix}_{21\times 21} + \begin{bmatrix} [0]_{2(n-1)\times 2(n-1)} & [0]_{2(n-1)\times(23-2n)} \\ [0]_{(23-2n)\times 2(n-1)} & k_2 \end{bmatrix}_{21\times 21} \tag{10}$$

where k_1 and k_2 are

$$k_1 = \begin{bmatrix} k_{\mathrm{P}} & 0 & -k_{\mathrm{P}} \\ 0 & 0 & 0 \\ -k_{\mathrm{P}} & 0 & k_{\mathrm{P}} + k_{\mathrm{N}} \end{bmatrix}_{3\times 3} \tag{11}$$

$$k_2 = \begin{bmatrix} k_{\mathrm{N}} & [0]_{1\times(21-2n)} & -k_{\mathrm{N}} \\ [0]_{(21-2n)\times 1} & & \\ -k_{\mathrm{N}} & & [0]_{(22-2n)\times(22-2n)} \end{bmatrix}_{(23-2n)\times(23-2n)} \tag{12}$$

When the negative stiffness element is connected to the ground, the stiffness matrix of the wind turbine with KDamper is

$$\boldsymbol{K}_{\mathbf{c}} = \begin{bmatrix} \boldsymbol{K}_{\mathbf{wc}} & [0]_{20\times 1} \\ [0]_{1\times 20} & 0 \end{bmatrix}_{21\times 21} + \begin{bmatrix} [0]_{18\times 18} & [0]_{18\times 3} \\ [0]_{3\times 18} & k_1 \end{bmatrix}_{21\times 21} \tag{13}$$

The mass, damping, and stiffness matrices of the wind turbine with control all have a size of 21 by 21 as an additional DOF is introduced by the transverse movement of the auxiliary mass.

3. Optimal design of KDamper and TMD

The following parameters are defined to design KDamper and TMD and evaluate and compare their control performances:

(1) Mass ratio (μ), which is the ratio of the auxiliary mass to the mass of the wind turbine. As passive control devices, increasing the mass ratio of KDamper and TMD can improve the vibration control effectiveness, but with further increasing the mass ratio, the improvement is marginal. Considering the practical allowable space within the nacelle and at the tower top, a mass ratio of 2% is assumed for both KDamper and TMD.

(2) Negative stiffness ratio (R_k), which is defined as $R_k = -k_{\mathrm{N}}/(k_{\mathrm{N}} + k_{\mathrm{P}})$. Similar to the mass ratio, previous studies have confirmed that a larger negative stiffness ratio provided better vibration isolation performance, however, which also caused issues of structural stability and manufacturing difficulty. In the present study, three different negative stiffness ratios are considered, namely 0.5, 1.0, and 1.5, and KDamper is optimized in these three ratios, respectively.

(3) Frequency ratio, which is defined as $f_{\mathrm{KD}} = \sqrt{(k_{\mathrm{P}} + k_{\mathrm{N}})/m_{\mathrm{D}}}/\omega_{\mathrm{s}}$ for KDamper and $f_{\mathrm{T}} = \sqrt{k_{\mathrm{P}}/m_{\mathrm{D}}}/\omega_{\mathrm{s}}$ for TMD, where ω_{s} is the natural frequency corresponding to the controlled mode of the wind turbine. Once the optimal frequency ratio is determined, the stiffness of the positive and negative spring elements of KDamper and the stiffness of the positive spring element of TMD can be obtained.

(4) Damping ratio, which is defined as $\zeta_{\mathrm{KD}} = c_{\mathrm{D}}/2\sqrt{m_{\mathrm{D}}(k_{\mathrm{P}} + k_{\mathrm{N}})}$ for KDamper and $\zeta_{\mathrm{T}} = c_{\mathrm{D}}/2\sqrt{m_{\mathrm{D}}k_{\mathrm{P}}}$ for TMD. The damping ratio is defined to determine the optimal dashpot coefficients for both KDamper and TMD.

Given that the control objective is to minimize the mean square displacement at the tower top, the frequency and damping ratios of KDamper and TMD are optimized exclusively to the first vibration mode of the wind turbine (i.e., $\omega_{\mathrm{s}} = 2.11$ rad/s). Moreover, the responses of the wind turbine with control can be described in the frequency domain by (Datta, 2010)

$$\boldsymbol{X}(\omega) = \boldsymbol{H}(i\omega)\boldsymbol{P}(\omega) \tag{14}$$

where $\boldsymbol{X}(\omega)$ is the response vector, $\boldsymbol{H}(i\omega)$ is the transfer function matrix, and $\boldsymbol{P}(\omega)$ is the external excitation vector. The transfer function and external excitation vector are calculated by (Datta, 2010)

$$\boldsymbol{H}(i\omega) = \left[\boldsymbol{K}_{\mathbf{c}} - \boldsymbol{M}_{\mathbf{c}}\omega^2 + i\boldsymbol{C}_{\mathbf{c}}\omega\right]^{-1} \tag{15}$$

$$\boldsymbol{P}(\omega) = -\boldsymbol{M}_{\mathbf{c}}\boldsymbol{I}\ddot{x}_g(\omega) \tag{16}$$

where $i^2 = -1$; $\ddot{x}_g(\omega)$ is the seismic motion in the frequency domain; $\boldsymbol{I}$ is the influence coefficient matrix, which is 1 corresponding to the translational DOFs and 0 corresponding to the rotational DOFs. The power spectral density (PSD) of the external excitation is thus (Datta, 2010)

$$\boldsymbol{S}_{\boldsymbol{pp}}(\omega) = \boldsymbol{M}_{\mathbf{c}}\boldsymbol{I}(\boldsymbol{M}_{\mathbf{c}}\boldsymbol{I})^T S_{\ddot{x}_g}(\omega) \tag{17}$$

where the superscript "T" denotes the matrix transposition; $S_{\ddot{x}_g}(\omega)$ is the PSD of ground motion acceleration and is assumed as white noise (S_0) in the present study. Having obtained the transfer function and the PSD of the external excitation, the PSD of the wind turbine response is given by (Datta, 2010)

$$\boldsymbol{S}_{\boldsymbol{xx}}(\omega) = \boldsymbol{H}(i\omega)\boldsymbol{S}_{\boldsymbol{pp}}(\omega)\boldsymbol{H}(i\omega)^{*T} \tag{18}$$

where the superscript "*" indicates a complex conjugate. Therefore, the mean square displacement at the tower top (corresponding to the 19th DOF) can be calculated by

$$\sigma^2_{x,19} = \int_{-\infty}^{+\infty} \boldsymbol{S}_{\boldsymbol{xx}}(19, 19)d\omega \tag{19}$$

Substituting the mass, damping, and stiffness matrices of the wind turbine with control in Section 2.3 into the above equations, it is observed that the mean square displacement at the tower top is only dependent on two variables: the defined frequency ratio and damping ratio. Two commonly used methods for optimising TMD are H_∞ and H_2 (Soltani and Deraemaeker, 2022). The H_∞ method involves optimising TMD parameters to minimize the peak amplitude in the frequency response function curve of the protected structure. This optimisation can be accomplished using the fixed point method (Den Hartog, 1947), which was also employed by Ikago et al. (2012) to optimally design a tuned viscous mass damper. On the other hand, the H_2 method focuses on designing TMD to minimize the mean square response of the protected structure, represented by the area under the frequency response function curve. H_∞ and H_2 are typically suitable for harmonic and random excitations, respectively. Given that seismic load is a random excitation in

Table 4
Optimal parameters of TMD.

Frequency ratio f_{T}	Spring stiffness (N/m)	Damping ratio ζ_{T}	Dashpot coefficient (N/(m/s))
0.951	56,142	0.092	5149

Table 5
Optimal parameters of KDamper when $R_k = 0.5$.

Location	Frequency ratio f_{KD}	Positive spring stiffness k_P (N/m)	Negative spring stiffness k_N (N/m)	Damping ratio ζ_{KD}	Damping coefficient c_D (N/(m/s))
m_9	0.950	84,036	−28,012	0.099	5535
m_8	0.948	83,682	−27,894	0.107	5970
m_7	0.947	83,506	−27,835	0.113	6298
m_6	0.945	83,153	−27,718	0.119	6618
m_5	0.943	82,802	−27,601	0.125	6937
m_4	0.941	82,451	−27,484	0.129	7144
m_3	0.940	82,276	−27,425	0.132	7303
m_2	0.939	82,101	−27,367	0.135	7461
m_1	0.938	81,926	−27,309	0.136	7508
Ground	0.938	81,926	−27,309	0.137	7563

Table 6
Optimal parameters of KDamper when $R_k = 1.0$.

Location	Frequency ratio f_{KD}	Positive spring stiffness k_P (N/m)	Negative spring stiffness k_N (N/m)	Damping ratio ζ_{KD}	Damping coefficient c_D (N/(m/s))
m_9	0.949	111,812	−55,906	0.107	5976
m_8	0.946	111,106	−55,553	0.122	6792
m_7	0.943	110,402	−55,201	0.136	7548
m_6	0.940	109,701	−54,850	0.148	8188
m_5	0.937	109,002	−54,501	0.159	8768
m_4	0.933	108,073	−54,037	0.168	9225
m_3	0.930	107,379	−53,690	0.175	9578
m_2	0.928	106,918	−53,459	0.180	9831
m_1	0.927	106,688	−53,344	0.184	10,038
Ground	0.926	106,458	−53,229	0.185	10,082

Table 7
Optimal parameters of KDamper when $R_k = 1.5$.

Location	Frequency ratio f_{KD}	Positive spring stiffness k_P (N/m)	Negative spring stiffness k_N (N/m)	Damping ratio ζ_{KD}	Damping coefficient c_D (N/(m/s))
m_9	0.948	139,470	−83,682	0.115	6416
m_8	0.945	138,589	−83,153	0.137	7619
m_7	0.941	137,418	−82,451	0.159	8806
m_6	0.936	135,962	−81,577	0.178	9805
m_5	0.931	134,513	−80,708	0.196	10,739
m_4	0.926	133,072	−79,843	0.210	11,445
m_3	0.921	131,639	−78,983	0.221	11,979
m_2	0.918	130,783	−78,470	0.230	12,426
m_1	0.916	130,213	−78,128	0.235	12,669
Ground	0.915	129,929	−77,958	0.236	12,709

the present study, the H_2 method is adopted to optimise both KDamper and TMD. Consequently, the mean square displacement at the tower top (Eq. (19)) is defined as the objective function to optimise the frequency and damping ratios of KDamper and TMD under the given parameters of the wind turbine, mass ratio, and negative stiffness ratio. In the present study, this optimisation problem is solved using the numerical searching method in MATLAB, a commonly employed approach for damper optimisation. The lower limits for frequency and damping ratios are defined as 0.1 and 0, respectively, with upper limits set as 2 and 1, respectively. Both frequency and damping ratios are explored within intervals of 0.001. Once these ratios are determined, the stiffness and damping coefficients of KDamper and TMD can be calculated using the equations outlined in this section. The results of the optimal parameters for TMD are presented in Table 4, and the corresponding results for KDamper with different negative stiffness ratios are given in Tables 5–7. It can be seen that the optimal frequency ratio slightly decreases, and the optimal damping ratio increases with connecting the negative stiffness spring element close to the tower base. In addition, with increasing the negative stiffness ratio, the frequency ratio decreases, and the damping ratio increases.

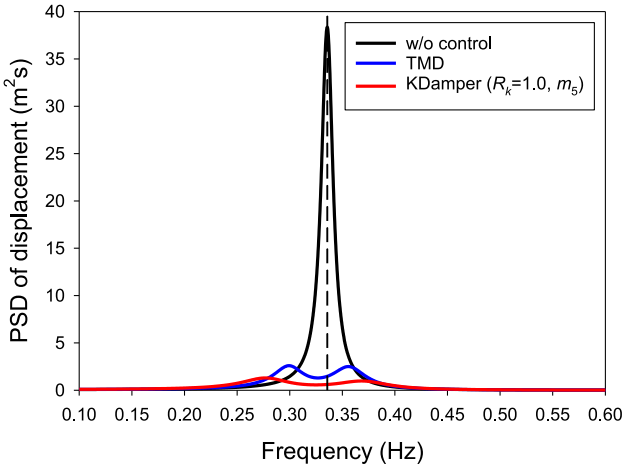

Fig. 6. PSD of the displacement at the tower top without and with control.

Table 8
Mean square displacements of the towers without control and with TMD.

Without control	With TMD	
Mean square displacement (m^2)	Mean square displacement (m^2)	Reduction ratio (%)
0.5383	0.1809	66.40

Table 9
Mean square displacements of the towers with KDamper when $R_k = 0.5$.

Location	Mean square displacement (m^2)	Reduction ratio compared to the original system (%)	Reduction ratio compared to TMD (%)
m_9	0.1709	68.25	5.51
m_8	0.1626	69.79	10.08
m_7	0.1559	71.03	13.79
m_6	0.1506	72.02	16.72
m_5	0.1465	72.78	18.99
m_4	0.1434	73.36	20.71
m_3	0.1412	73.78	21.96
m_2	0.1396	74.06	22.80
m_1	0.1387	74.23	23.28
Ground	0.1385	74.28	23.44

Table 10
Mean square displacements of the towers with KDamper when $R_k = 1.0$.

Location	Mean square displacement (m^2)	Reduction ratio compared to the original system (%)	Reduction ratio compared to TMD (%)
m_9	0.1621	69.89	10.39
m_8	0.1481	72.49	18.12
m_7	0.1378	74.41	23.83
m_6	0.1302	75.81	28.00
m_5	0.1248	76.83	31.03
m_4	0.1208	77.55	33.18
m_3	0.1181	78.05	34.68
m_2	0.1164	78.38	35.65
m_1	0.1154	78.56	36.20
Ground	0.1151	78.62	36.37

Table 11
Mean square displacements of the towers with KDamper when $R_k = 1.5$.

Location	Mean square displacement (m^2)	Reduction ratio compared to the original system (%)	Reduction ratio compared to TMD (%)
m_9	0.1542	71.35	14.74
m_8	0.1362	74.69	24.67
m_7	0.1240	76.96	31.42
m_6	0.1157	78.51	36.04
m_5	0.1100	79.57	39.19
m_4	0.1061	80.28	41.31
m_3	0.1036	80.75	42.72
m_2	0.1020	81.05	43.60
m_1	0.1011	81.21	44.08
Ground	0.1009	81.26	44.23

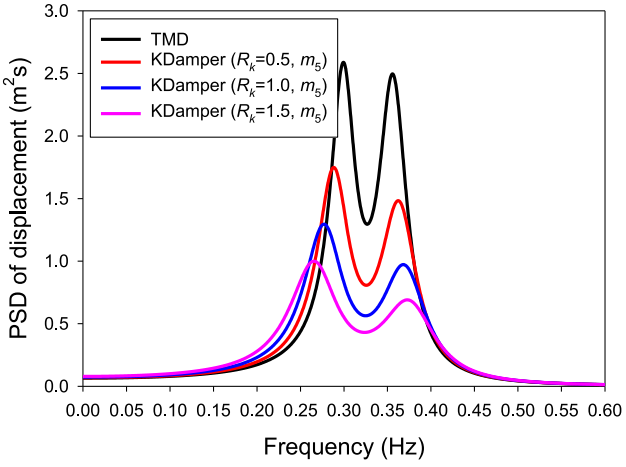

Fig. 7. PSD of the displacement at the tower top with KDamper connected to m_5 and various negative stiffness ratios.

4. Frequency domain analyses

The responses of the wind turbines without and with control in the frequency domain are investigated under a unit white noise intensity in this section. In particular, the PSD of the translational displacement at the tower top is taken out from Eq. (18) for demonstration. The control effectiveness of KDamper is compared to the traditional TMD, and the effectiveness between different KDamper configurations is also compared.

Fig. 6 shows the PSD of the displacement at the tower top without and with control. For conciseness, only one KDamper with a negative stiffness ratio of 1.0 and connected to m_5 (i.e., a height of 43.80 m above the ground) is presented. The maximum value represents the resonant amplitude of the uncontrolled tower (the black curve) and occurs at a frequency of 0.3357 Hz, corresponding to the first natural frequency of the tower. Generally, after the installation of control devices (KDamper and TMD), the tower responses are significantly reduced, with much lower values. To provide a quantitative comparison of the control effectiveness between KDamper and TMD, the mean square displacements of the uncontrolled and controlled towers are tabulated in Tables 8–11. The corresponding reductions of the mean square displacements between the towers without control, and with KDamper and TMD are also given in these tables. As shown in Table 8, the mean square displacement of the uncontrolled tower is 0.5383 m^2, and it is reduced to 0.1809 m^2 with a reduction ratio of 66.40% when TMD is applied.

Furthermore, as presented in Tables 9–11, KDamper provides larger reduction ratios of the mean square displacements than TMD, irrespective of which configuration is adopted, indicating that KDamper has superior control effectiveness. However, the effectiveness of KDamper is dependent on the negative stiffness ratio and which mass point the negative stiffness element is connected to. When the connected mass point is fixed, better control effectiveness is achieved by increasing the negative stiffness ratio. This can be explained by Fig. 7, where the PSD curves of the displacement at the tower top with KDamper connected to the mass point m_5 are compared among the considered negative stiffness ratios. As shown, a larger R_k value leads to a smaller under-curve area and thus a lower mean square displacement. In addition, with the same R_k used, the downward connection provides more effective vibration

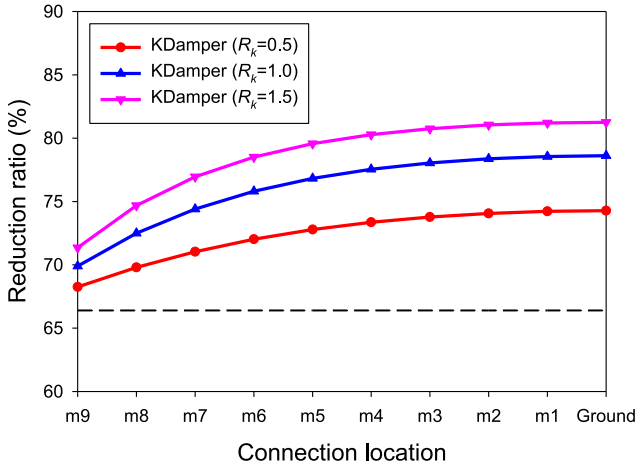

Fig. 8. Reduction ratios of mean square displacements under various connection locations and negative stiffness ratios.

Table 12
Information of earthquake ground motions.

No.	RSN	Earthquake event	Station	Magnitude	R_{rup} (km)	V_{s30} (m/s)	PGA (g)	Scaling factor
1	6	Imperial Valley-02	El Centro Array #9	6.95	6.09	213.44	0.281	1.7192
2	15	Kern County	Taft Lincoln School	7.36	38.89	385.43	0.159	3.4474
3	169	Imperial Valley-06	Delta	6.53	22.03	242.05	0.236	1.8987
4	173	Imperial Valley-06	El Centro Array #10	6.53	8.60	202.85	0.173	2.3431
5	180	Imperial Valley-06	El Centro Array #5	6.53	3.95	205.63	0.529	1.2973
6	182	Imperial Valley-06	El Centro Array #7	6.53	0.56	210.51	0.341	1.4696
7	728	Superstition Hills-02	Westmorland Fire Station	6.54	13.03	193.67	0.173	2.6204
8	779	Loma Prieta	LGPC	6.93	3.88	594.83	0.570	0.5825
9	799	Loma Prieta	SF Intern. Airport	6.93	58.65	190.14	0.236	2.2179
10	900	Landers	Yermo Fire Station	7.28	23.62	353.63	0.245	1.8006
11	984	Northridge-01	LA - 116th St School	6.69	41.17	301.00	0.208	4.2034
12	1044	Northridge-01	Newhall Fire Station	6.69	5.92	269.14	0.583	0.9268
13	1107	Kobe, Japan	Kakogawa	6.90	22.50	312.00	0.240	2.5444
14	1120	Kobe, Japan	Takatori	6.90	1.47	256.00	0.618	0.5334
15	1540	Chi-Chi, Taiwan	TCU115	7.62	21.76	215.34	0.096	3.2658
16	1633	Manjil, Iran	Abbar	7.37	12.55	723.95	0.515	1.5303
17	5618	Iwate, Japan	IWT010	6.90	16.27	825.83	0.226	2.3271
18	6890	Darfield, New Zealand	Christchurch Cashmere High School	7.00	17.64	204.00	0.229	1.6975

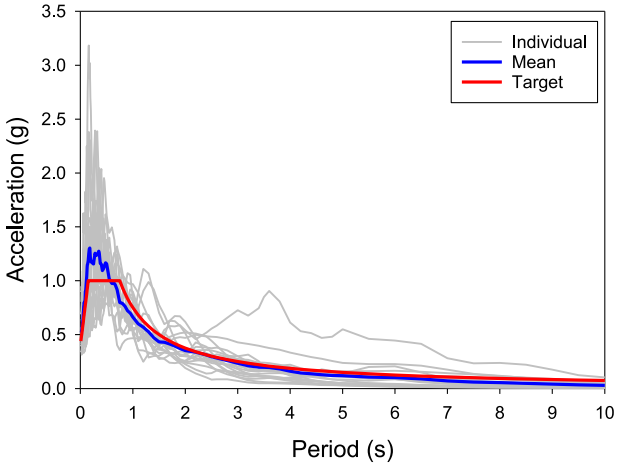

Fig. 9. Acceleration response spectra.

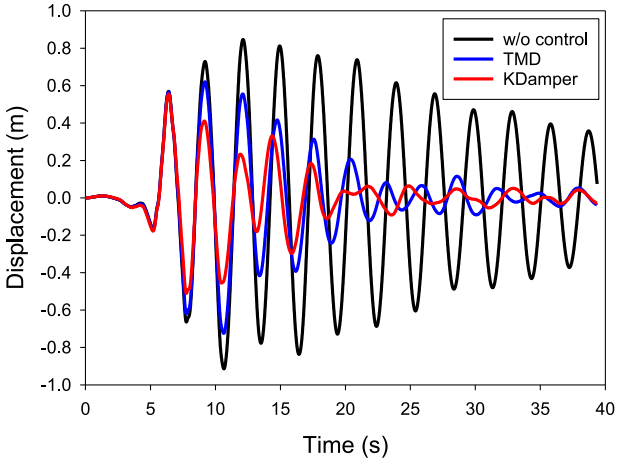

Fig. 10. Displacements at the tower top under the No. 5 seismic motion.

control, but the improvement of control effectiveness by connecting to mass further downward towards the tower base is marginal. Fig. 8 illustrates the variations of the mean square displacement reduction ratios with respect to different KDamper connections, and the reduction ratio achieved by TMD is also presented for comparison (the black dashed line). As shown, the mean square displacement of the tower is significantly reduced when KDamper is connected from m_9 to m_5, but the reduction ratio does not change too much when KDamper is connected from m_5 to the ground. For example, when the negative stiffness ratio is 1.5, the mean square displacements are reduced by 71.35%, 79.57%, and 81.26% when connected to m_9, m_5, and the ground, respectively, and only an improvement of 1.69% is achieved from the further downward connection from m_5 to the ground. Similar findings for $R_k = 0.5$ and $R_k = 1.0$ can be found in Tables 9 and 10 and Fig. 8. The reason is that the structural displacements below m_5 are not substantial, and they are also considerably mitigated by KDamper. Consequently, the negative stiffness connected below m_5 is unable to exert more effective control. To balance the control effectiveness and practical feasibility, KDamper with a negative stiffness ratio of 1.5 and connected to m_5 is selected to carry out seismic response analyses in the time domain in the following section.

5. Time domain analyses

5.1. Seismic motion selection

To systematically examine the control performances of KDamper with a negative stiffness ratio of 1.5 and connected to m_5, a total of 18 earthquake ground motions are selected and downloaded from the PEER ground motion database, and their detailed information is given in Table 12. Moreover, these seismic motions are scaled to match the acceleration response spectrum with a structural damping ratio of 5% outlined in study of ASCE (2010). Fig. 9 shows the acceleration response spectra of these seismic motions, and their mean spectrum agrees well with the target spectrum.

5.2. Displacement responses at the tower top

Fig. 10 shows the displacement time histories at the top of the tower for both uncontrolled and controlled scenarios when subjected to the No. 5 seismic motion, and the displacement responses under the other seismic motions are presented in the appendix (Fig. A1).

Compared to the tower without control, the displacement responses at the tower top are quickly damped out by KDamper and TMD, but the reductions are different under different seismic motions because of the inherent stochastic characteristics of earthquakes. To provide a

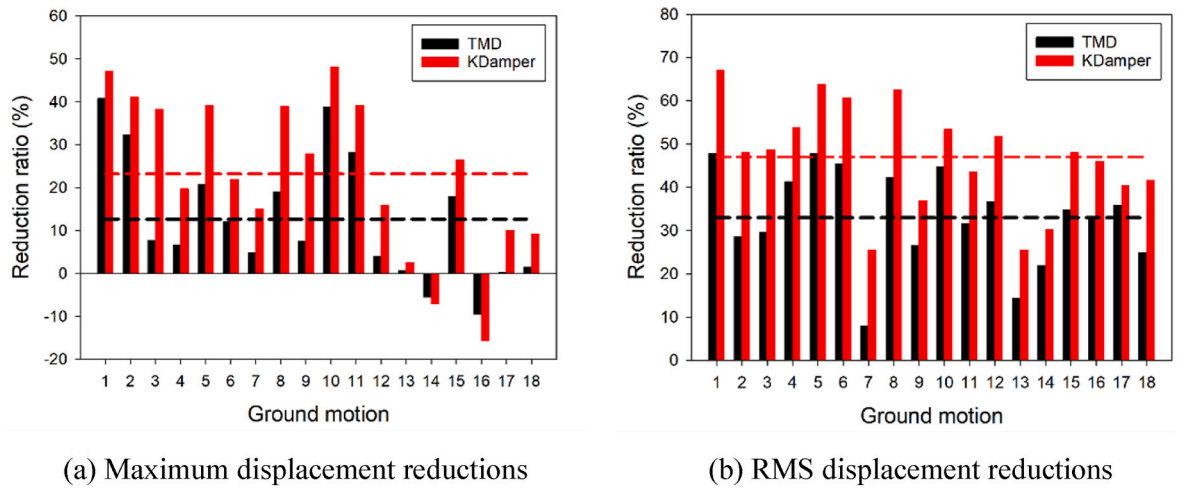

Fig. 11. Reduction ratios of maximum and RMS displacements.

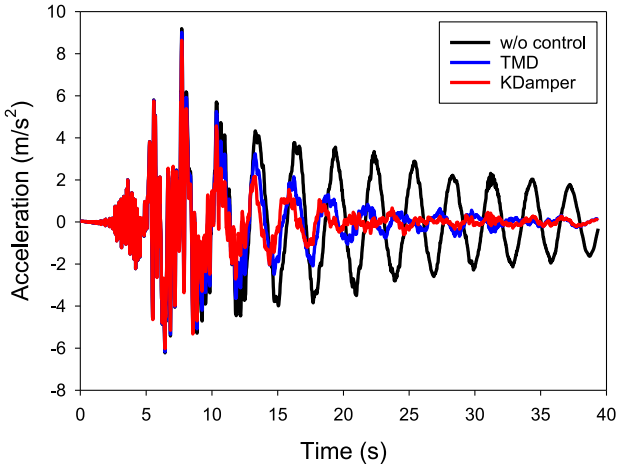

Fig. 12. Accelerations at the tower under the No. 5 seismic motion.

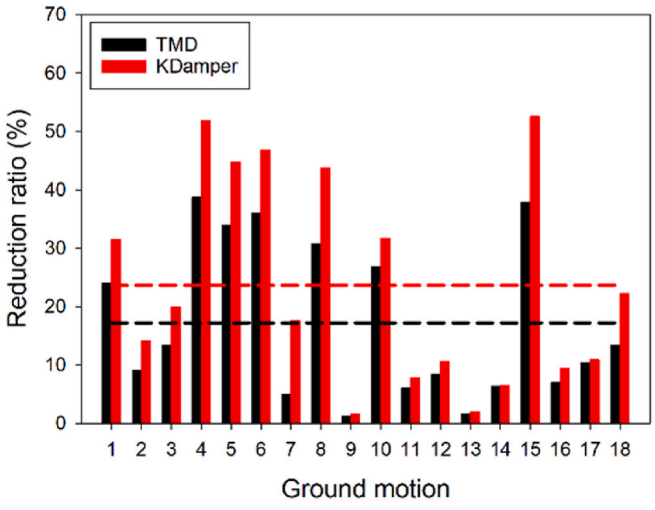

Fig. 13. Reduction ratios of RMS accelerations.

comprehensive evaluation of the control effectiveness of KDamper and TMD, Fig. 11 presents the reduction ratios of the maximum displacement and root mean square (RMS) displacement at the tower top between controlled and uncontrolled systems.

The average reduction ratio of the maximum displacement at the tower top with KDamper is approximately 23% (the red dashed line in Fig. 11(a)), which is 10% larger than that of TMD (the black dashed line), indicating that both KDamper and TMD can effectively reduce the maximum displacement and KDamper outperforms its counterpart TMD. However, it should be noted that the control effect of KDamper and TMD in reducing the peak displacement is opposite when the wind turbine is exposed to the Nos. 13, 14, and 16 seismic motions as the peak displacement is even increased under the Nos. 14 and 16 seismic motions. When subjected to the ground motion No. 13, the control effectiveness is not evident. This can be explained as follows: (1) It is attributed to the occurrence time of the maximum displacement, which is in the initial stage of the displacement time histories for the above seismic motions as illustrated in Fig. A1, and the control effect is marginal. To achieve effective control, the relative motion between the tower and the control devices should develop, and it requires a certain amount of time for the control devices to respond and generate relative motion. (2) A variety of factors that challenge the effectiveness of control devices. Primarily, these involve the potential for resonance and

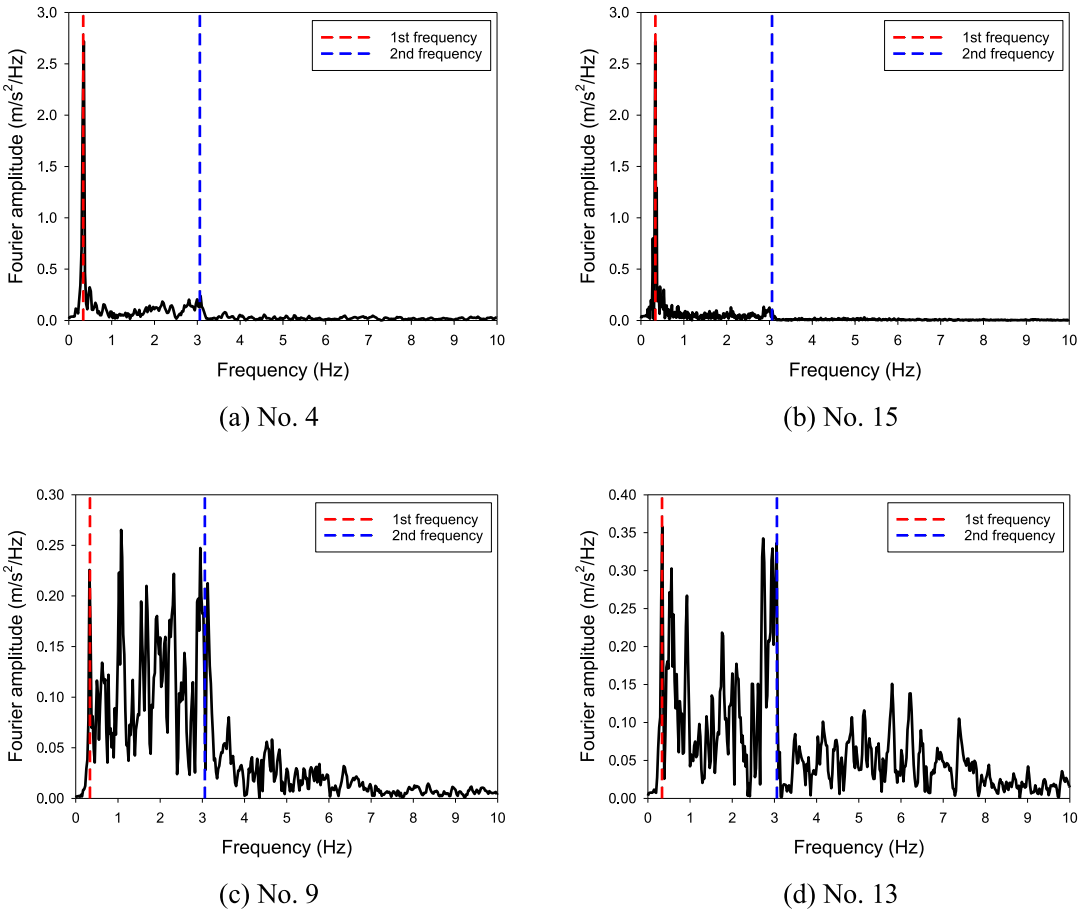

Fig. 14. Acceleration Fourier spectra of the uncontrolled tower under Nos. 4, 15, 9, and 13 seismic motions.

Table 13
Average RMS displacements and accelerations under different structural frequency ratios.

Frequency ratio	RMS displacement (m)			RMS acceleration (m/s^2)		
	Uncontrolled	KDamper	TMD	Uncontrolled	KDamper	TMD
−30%	0.3082	0.2076	0.2751	1.1871	0.9942	1.1162
−25%	0.3461	0.1776	0.2822	1.3263	0.9818	1.1703
−20%	0.3586	0.1591	0.2859	1.4642	1.0009	1.2548
−15%	0.3082	0.1485	0.2563	1.4261	1.0244	1.2652
−10%	0.2577	0.1392	0.2073	1.3564	1.0500	1.2143
−5%	0.2555	0.1302	0.1728	1.4478	1.0733	1.1866
0%	0.2525	0.1230	0.1602	1.5339	1.0886	1.2091
5%	0.2543	0.1182	0.1596	1.6447	1.1199	1.2732
10%	0.2529	0.1151	0.1579	1.7120	1.1303	1.2983
15%	0.2213	0.1131	0.1535	1.6393	1.1706	1.3380
20%	0.2008	0.1125	0.1504	1.6161	1.2132	1.3801
25%	0.1871	0.1136	0.1489	1.6118	1.2515	1.4246
30%	0.1847	0.1150	0.1532	1.6975	1.3072	1.5263

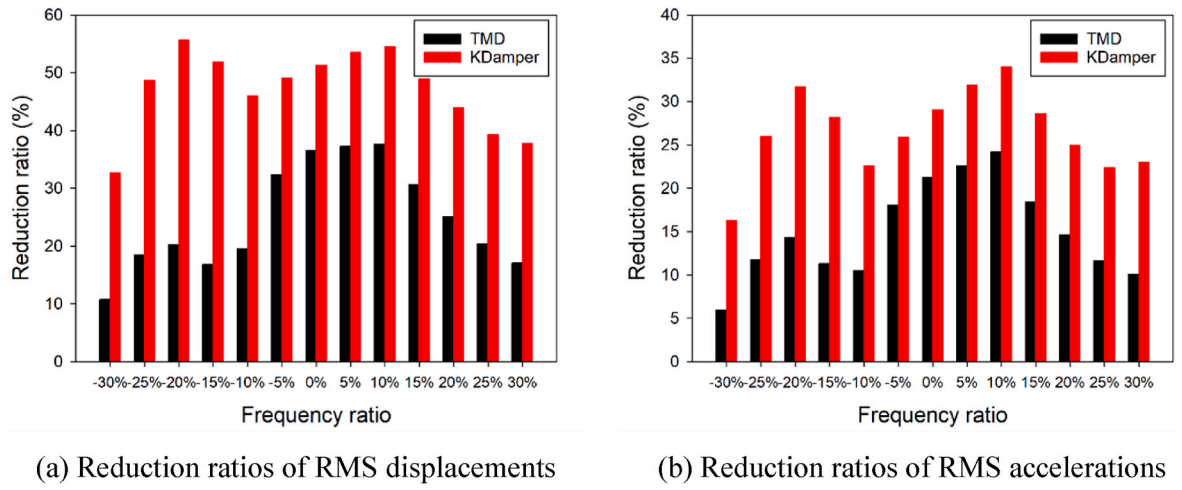

Fig. 15. Reduction ratios of the average RMS displacements and accelerations under different frequency ratios.

inappropriate tuning. Resonance can occur when the frequency of seismic motion aligns not with the natural frequency of the protected structure but with that of the control device, resulting in an increase in energy in the system and thus amplified displacement. Meanwhile, inappropriate tuning arises when the devices' parameters do not align optimally with the frequency of the seismic event, potentially leading to an inadvertent addition of energy to the system, again causing an increase in displacement.

Compared to the maximum displacement reduction, KDamper and TMD are more effective in reducing the RMS displacement at the top of the tower. The average reduction ratios of the RMS displacement for the wind turbine equipped with KDamper and TMD are 47% and 33%, respectively, and KDamper performs better than TMD again.

5.3. Acceleration responses at the tower top

Many mechanical and electrical equipment of wind turbines are sensitive to accelerations and thus the control effect of KDamper on the acceleration responses is also investigated. Fig. 12 shows the acceleration time histories at the tower top without control and with KDamper and TMD when subjected to the No. 5 seismic motion, and the results for the other seismic motions are shown in the Appendix (Fig. A2). In addition, the reduction ratios of the RMS accelerations between the controlled and uncontrolled scenarios are presented in Fig. 13.

Similar to displacement reduction, the acceleration responses are considerably reduced by KDamper and TMD, and KDamper has a superior control effect than TMD under the examined seismic motions. Specifically, the average reduction ratios of the RMS accelerations achieved by KDamper and TMD are 24% and 17%, respectively. It is confirmed that KDamper's control ability in reducing the acceleration responses for different ground motion inputs is consistent with its effectiveness in reducing the RMS displacements, and KDamper is more effective than TMD for reducing the RMS accelerations and displacements of the wind turbine tower under seismic excitations. However, the reduction ratios of the RMS accelerations induced by KDamper are dependent on the seismic input, which can be explained by transforming the acceleration responses of the uncontrolled tower from the time domain to the frequency domain. Fig. 14 shows the Fourier spectra of the accelerations at the tower top when subjected to the Nos. 4, 9, 13, and 15 seismic motions, as KDamper performs the best in reducing the RMS accelerations under the Nos. 4 and 15 seismic motions while it is the worst under the Nos. 9 and 13 seismic motions. As shown in Fig. 14 (a) and (b), the largest Fourier amplitude occurs at a frequency of 0.33 Hz, which corresponds to the first natural frequency of the tower, indicating that the acceleration responses at the tower top are mainly contributed by the first vibration mode when the wind turbine is subjected to the Nos. 4 and 15 seismic motions. As mentioned above, both KDamper and TMD are tuned to control the first vibration mode of the tower, therefore, they have good control effectiveness under these two earthquake ground motions. However, when the wind turbine is excited by the Nos. 9 and 13 seismic motions, in addition to the first vibration mode, the second vibration mode of the tower is also excited, and the Fourier amplitudes at the first and second natural frequencies are almost the same, i.e., the acceleration responses are dominated by the first and second vibration modes. The second vibration mode cannot be effectively controlled by KDamper and TMD with the first natural frequency-oriented design, which leads to less than a 5% reduction in the RMS accelerations for these two excitations.

Moreover, the control device location is another factor that affects its control effectiveness, and it exerts optimal control by locating it at the maximum amplitude of the target mode. In the present study, both KDamper and TMD are placed at the tower top, which complies with the location of the maximum amplitude for the first mode. However, as shown in Fig. 3, the maximum amplitude of the second mode occurs approximately 40 m below the tower top. Therefore, when the second mode of the tower is excited by seismic loads such as the Nos. 9 and 13 seismic motions, KDamper and TMD installed at the tower top partially lose their control capability.

5.4. Robustness

Considering the natural frequency change of the wind turbine in the whole life period, the control robustness of KDamper is investigated by shifting the fundamental frequency of the tower from −30% to 30% of the original frequency with an interval of 5%. It should be noted that the frequency variation is realized by changing the elastic modulus of the tower, while the parameters of KDampers and TMD are kept the same as their optimal design.

Table 13 presents the average RMS displacements and accelerations at the tower top under different structural frequency ratios, i.e., the RMS results in this table are computed as the sum of the RMS responses under the examined seismic motions divided by the number of these seismic motions. Moreover, the reduction ratios of the average RMS displacements and accelerations between the controlled and uncontrolled towers are shown in Fig. 15. For comparison, the results corresponding to the original frequency (i.e., the frequency ratio of 0%) are also given in Table 13 and Fig. 15.

As shown in Table 13 and Fig. 15, in general, both KDamper and

TMD can control the RMS displacements and accelerations at the tower top when the frequency ratio is changed within a range of −30% to 30%, and KDamper outperforms TMD counterpart, indicating that KDamper is more robust against the structural frequency variation.

Specifically, when the structural frequency is unchanged, the average RMS displacements at the tower top with KDamper and TMD are 0.1230 m and 0.1602 m, respectively, and the corresponding reduction ratios are 51% and 37%. Two extreme cases of the frequency ratios are discussed here. When the structural frequency is 70% of the original frequency (i.e., a decrease of 30%), the average RMS displacements of KDamper and TMD are 0.2076 m and 0.2751 m with the reduction ratios of 33% and 11%, respectively. When the structural frequency is increased by 30%, the RMS displacements reduced by KDamper and TMD are 38% and 17%, respectively. Although the reduction ratios of the average RMS displacements achieved by KDamper are dependent on the structural frequency, they are larger than those of TMD and their variability is smaller than TMD. Similar observations can be found in the average RMS acceleration reductions by KDamper and TMD, which are not described in detail. In short, KDamper has control robustness in reducing the seismic responses of the wind turbine.

6. Conclusions

In the present study, KDamper is proposed to improve the seismic performances of wind turbines. The equations of motion of a wind turbine without and with control are developed. The parameters of KDamper are optimally designed by taking into account the connection location and the negative stiffness ratio. Both frequency and time domain analyses are conducted to investigate the control effectiveness of KDamper and compared to the traditional TMD. In addition, the control robustness of KDamper is also examined under different structural frequencies. The main conclusions are summarized as follows:

(1) Connecting the negative stiffness spring element close to the tower base and increasing the negative stiffness ratio leads to a slight decrease in the optimal frequency ratio of KDamper, accompanied by an increase in the optimal damping ratio.
(2) The effectiveness of KDamper in controlling vibrations depends on both the negative stiffness ratio and the connection location. A substantial negative stiffness ratio and a connection point near the tower base result in more effective control. However, the degree of improvement is limited when KDamper is connected below a height of 43.8 m.
(3) KDamper proves effective in mitigating both the maximum and RMS displacements of the wind turbine tower under the considered seismic motions, with a more pronounced impact on RMS displacements. Furthermore, KDamper demonstrates effective control over RMS accelerations. Specifically, the installation of KDamper results in a 47% reduction in RMS displacements and a 24% reduction in RMS accelerations. In comparison, TMD achieves a reduction of 33% in RMS displacements and 17% in RMS accelerations, highlighting the superior performance of KDamper. It is worth noting, however, that in scenarios where the maximum displacement occurs in the initial seconds or when higher vibration modes of the tower are excited by seismic loads, a single KDamper located at the tower top may partially lose its control capability.
(4) KDamper is more robust against changes in structural frequency compared to TMD. With a 30% increase in structural frequency, KDamper achieves reductions of 38% in average RMS displacements and 23% in RMS accelerations, as opposed to 17% and 10%, respectively, for TMD. Conversely, with a 30% decrease in structural frequency, KDamper achieves reductions of 33% in average RMS displacements and 16% in RMS accelerations, while TMD achieves lower reductions of 11% and 6%, respectively.

7. Discussions

The present study aims to introduce KDamper and investigate its feasibility and performance in controlling wind turbine responses under seismic motions only. Future research endeavours should address the following issues:

(1) The practical implementation of KDamper involves careful consideration of the wind turbine's design, structural dynamics, and the desired level of damping.
(2) Understanding the influences of seismic motion characteristics on wind turbine responses is critical. Moreover, KDamper not only targets seismic-induced vibrations but also offers potential benefits in mitigating wind-induced vibrations.
(3) Scaled experimental tests are crucial in validating the effectiveness of KDamper in mitigating vibrations in wind turbines.

Declaration of competing interest

The authors declare that they have no known competing financial interests or personal relationships that could have appeared to influence the work reported in this paper.

Acknowledgements

The authors would like to acknowledge the financial support from the Australian Research Council Future Fellowship (FT200100183) and the National Natural Science Foundation of China (No. 52108479). The second author gratefully acknowledges the financial support from the Curtin Research Stipend Scholarship.

Appendix A. Displacement and acceleration time histories

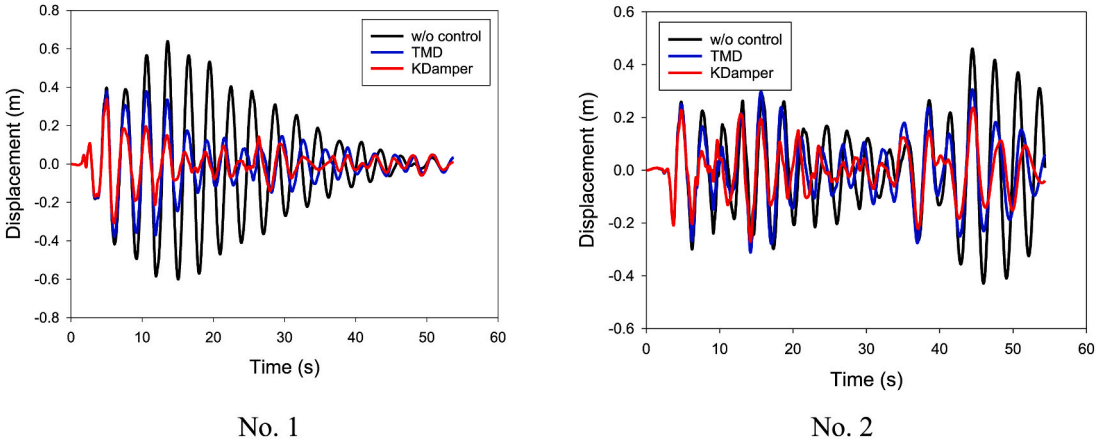

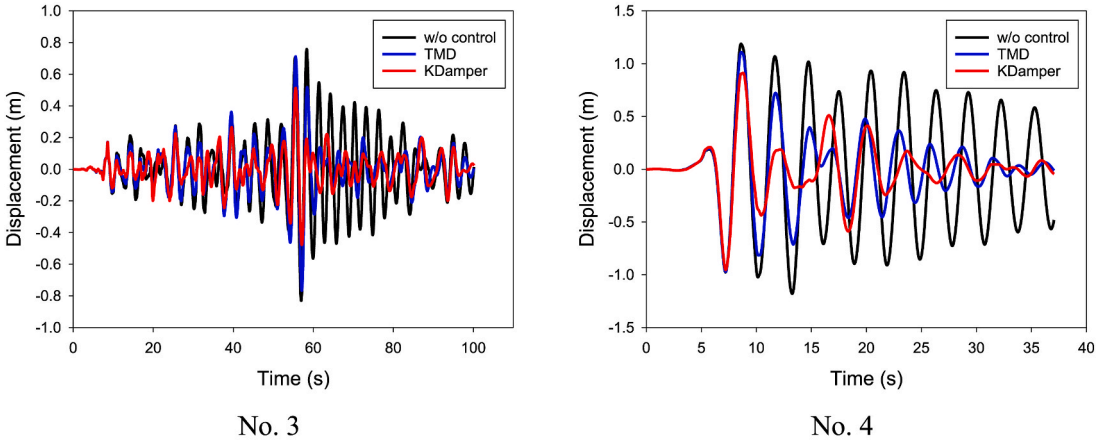

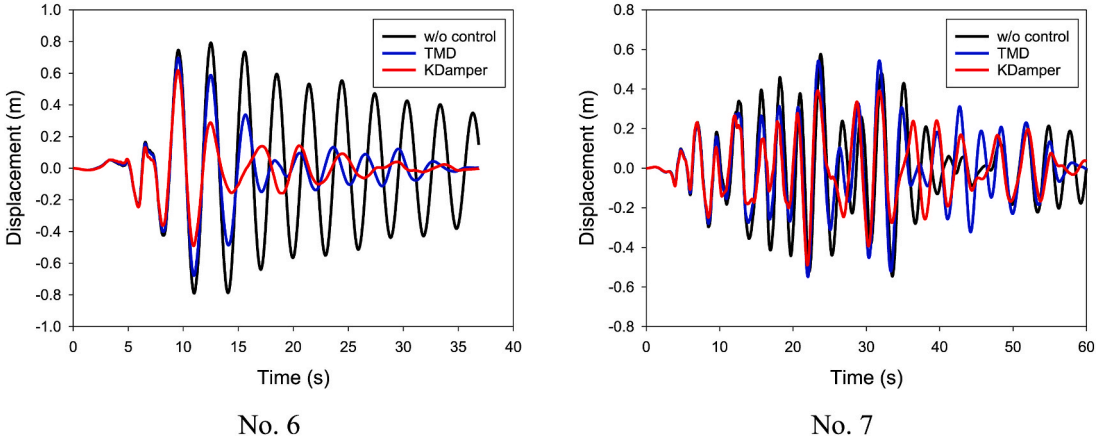

Fig. A1. Displacement time histories at the tower top with and without control.

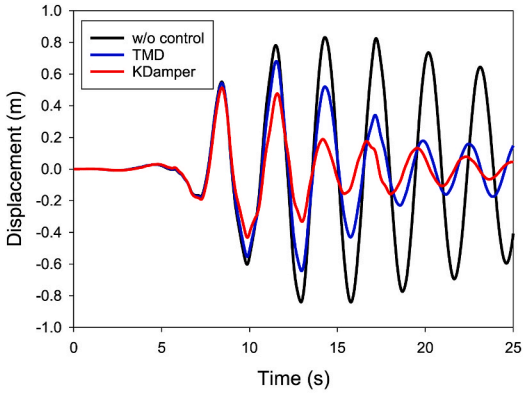

No. 8

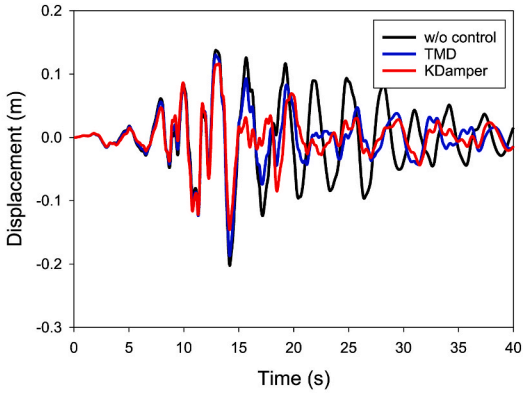

No. 9

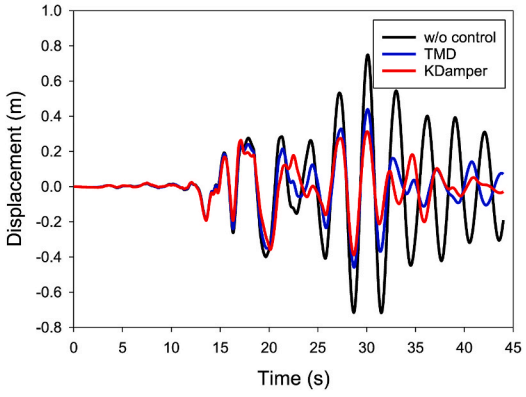

No. 10

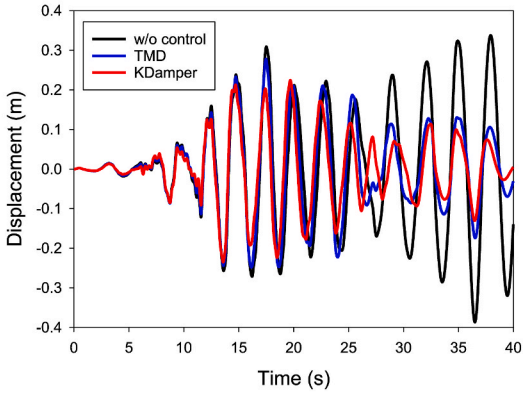

No. 11

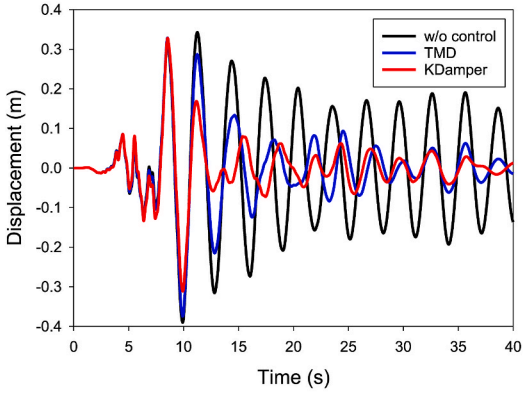

No. 12

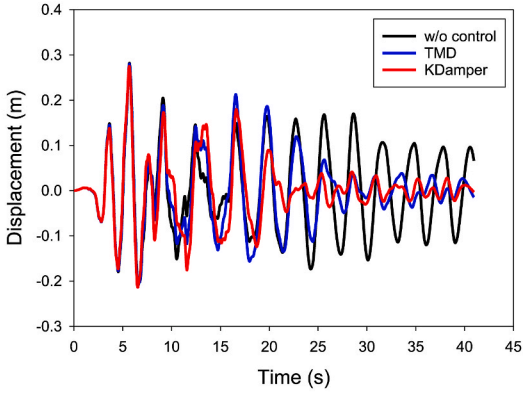

No. 13

Fig. A1. (*continued*).

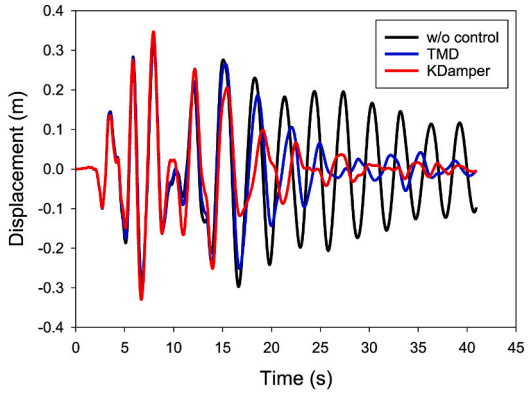

No. 14

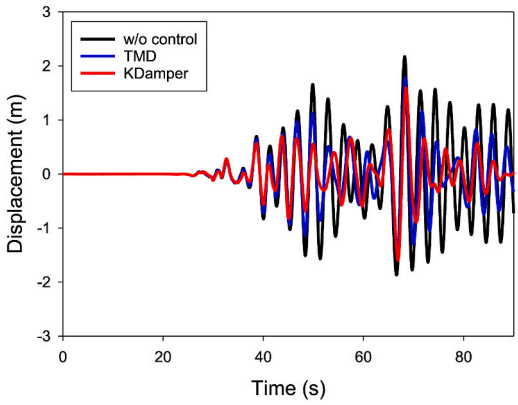

No. 15

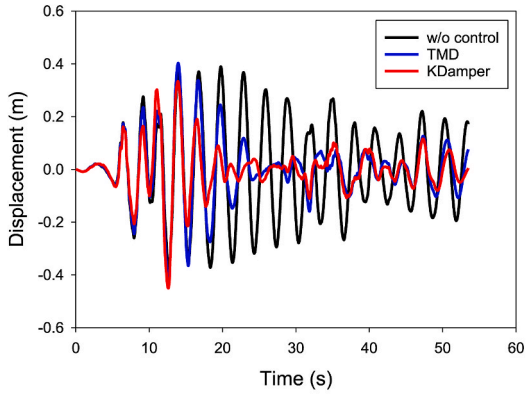

No. 16

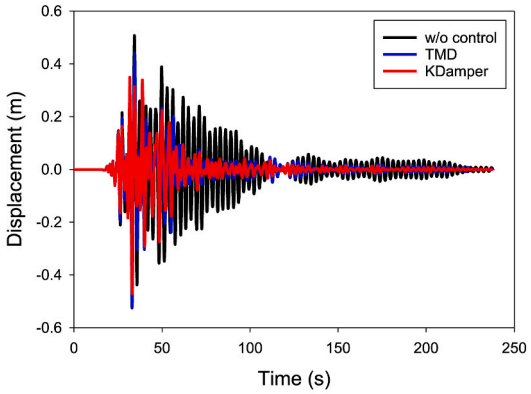

No. 17

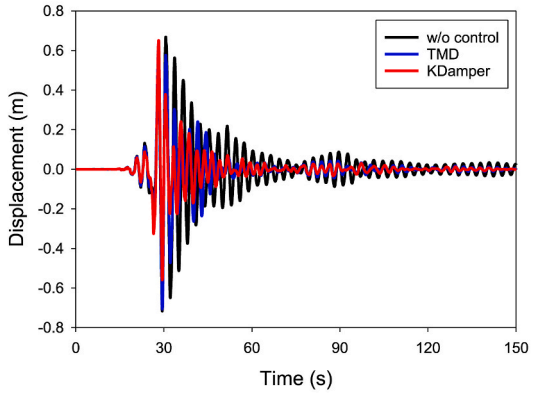

No. 18

Fig. A1. (*continued*).

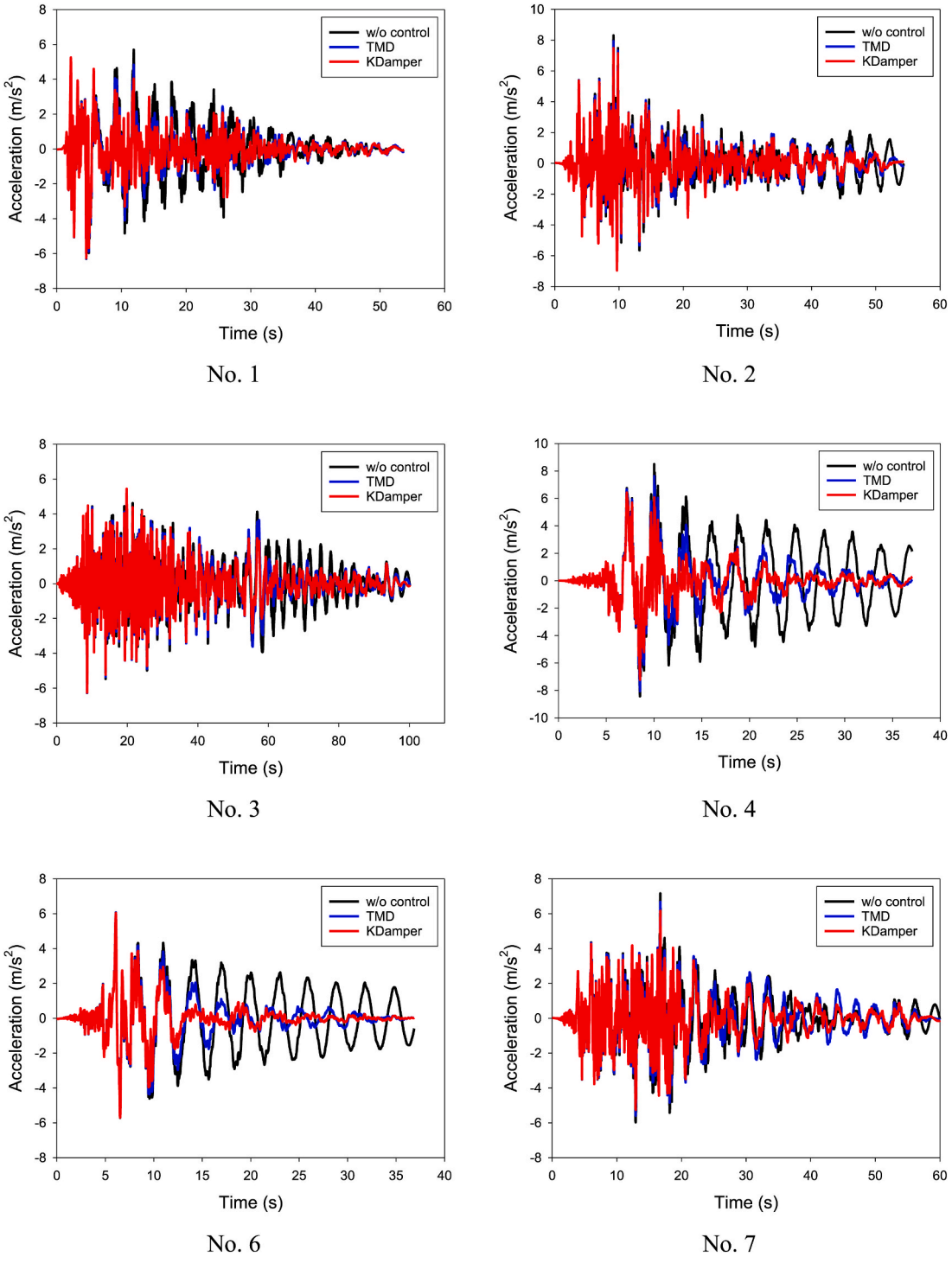

Fig. A2. Acceleration time histories at the tower top with and without control.

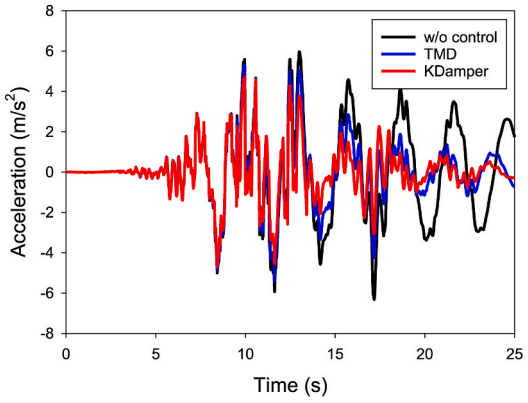

No. 8

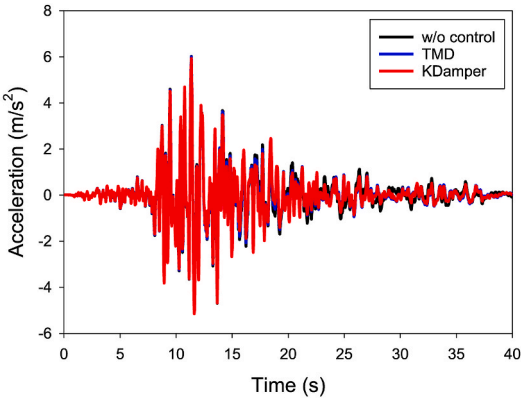

No. 9

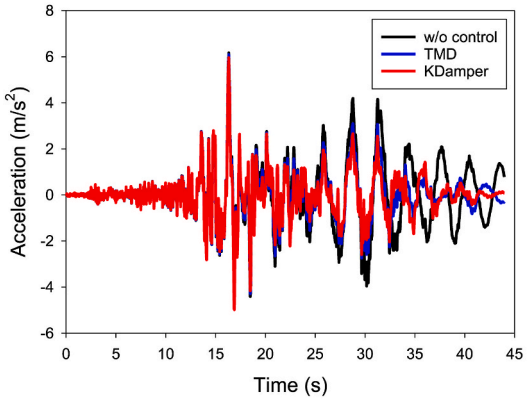

No. 10

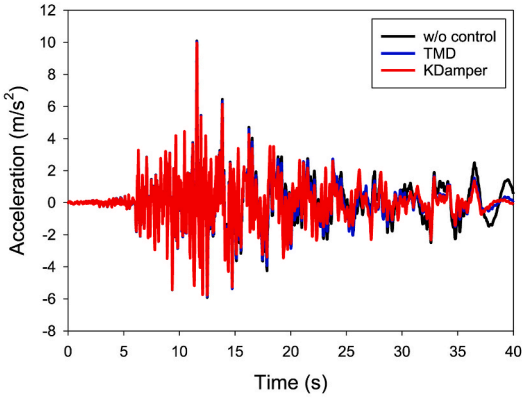

No. 11

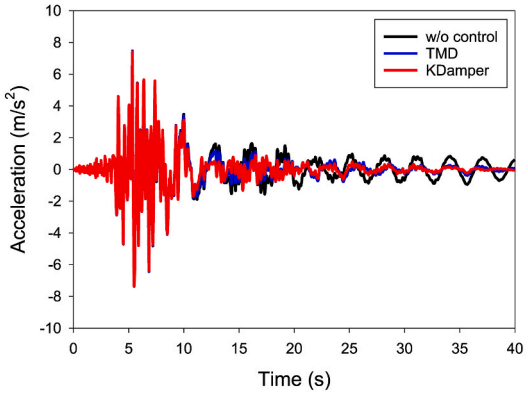

No. 12

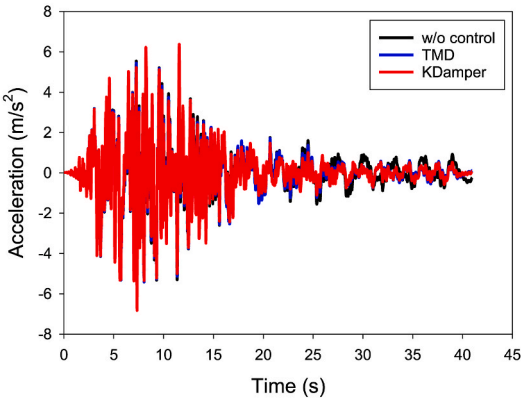

No. 13

Fig. A2. (*continued*).

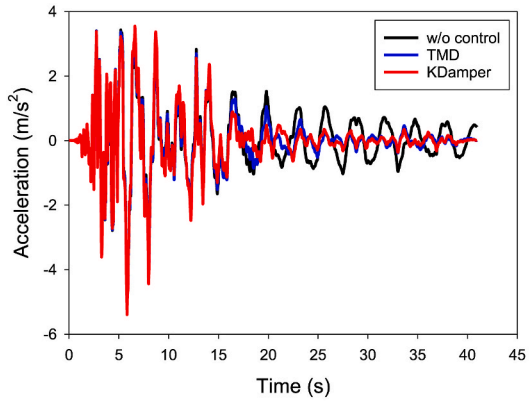

No. 14

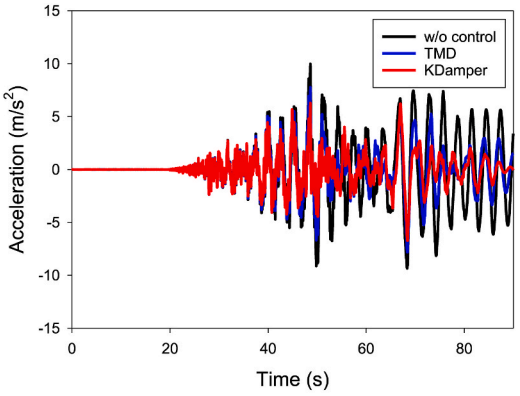

No. 15

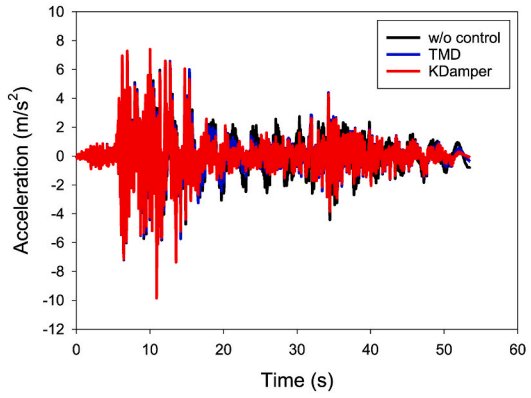

No. 16

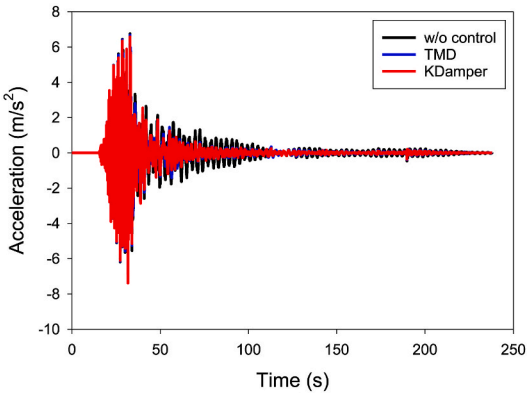

No. 17

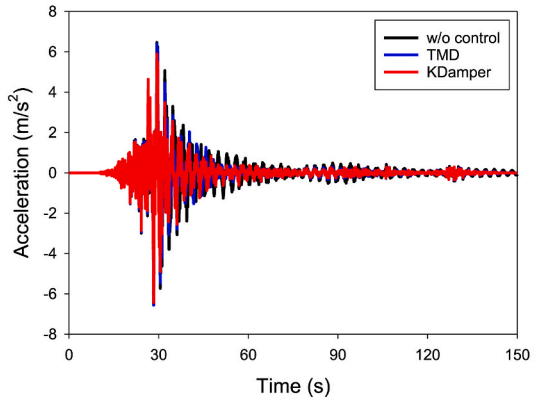

No. 18

Fig. A2. (*continued*).

References

Alkhoury, P., Aït-Ahmed, M., Soubra, A.-H., Rey, V., 2022. Vibration reduction of monopile-supported offshore wind turbines based on finite element structural analysis and active control. Ocean Eng. 263, 112234. https://doi.org/10.1016/j.oceaneng.2022.112234.

Antoniadis, I., Chronopoulos, D., Spitas, V., Koulocheris, D., 2015. Hyper-damping properties of a stiff and stable linear oscillator with a negative stiffness element. J. Sound Vib. 346, 37–52. https://doi.org/10.1016/j.jsv.2015.02.028.

Antoniadis, I.A., Kanarachos, S.A., Gryllias, K., Sapountzakis, I.E., 2018. KDamping: a stiffness based vibration absorption concept. J. Vib. Control 24, 588–606. https://doi.org/10.1177/1077546316646514.

ASCE, 2010. Minimum Design Loads for Buildings and Other Structures. American Society of Civil Engineers, USA.

Attary, N., Symans, M., Nagarajaiah, S., Reinhorn, A.M., Constantinou, M.C., Sarlis, A.A., Pasala, D.T., Taylor, D., 2015. Numerical simulations of a highway bridge structure employing passive negative stiffness device for seismic protection. Earthq. Eng. Struct. Dynam. 44, 973–995. https://doi.org/10.1002/eqe.2495.

Bernuzzi, C., Crespi, P., Montuori, R., Nastri, E., Simoncelli, M., Stochino, F., Zucca, M., 2021. Resonance of steel wind turbines: problems and solutions. Structures 32, 65–75. https://doi.org/10.1016/j.istruc.2021.02.053.

Brodersen, M.L., Bjørke, A.S., Høgsberg, J., 2017. Active tuned mass damper for damping of offshore wind turbine vibrations. Wind Energ. 20 (5), 783–796. https://doi.org/10.1002/we.2063.

Chapain, S., Aly, A.M., 2021. Vibration attenuation in wind turbines: a proposed robust pendulum pounding TMD. Eng. Struct. 233, 111891. https://doi.org/10.1016/j.engstruct.2021.111891.
Chen, D., Huang, S., Huang, C., Liu, R., Ouyang, F., 2021. Passive control of jacket-type offshore wind turbine vibrations by single and multiple tuned mass dampers. Mar. Struct. 77, 102938. https://doi.org/10.1016/j.marstruc.2021.102938.
Chen, J., Georgakis, C.T., 2013. Spherical tuned liquid damper for vibration control in wind turbines. J. Vib. Control 21 (10), 1875–1885. https://doi.org/10.1177/1077546313495911.
Chen, M.Z., Li, Z., Wang, H., Hu, Y., 2023. Seismic response mitigation of a wind turbine via inerter-based structural control. Bull. Earthq. Eng. 21, 1361–1388. http://doi.org/10.1007/s10518-021-01267-x.
Colherinhas, G.B., Girão De Morais, M.V., Machado, M.R., 2022. Spectral model of offshore wind turbines and vibration control by pendulum tuned mass dampers. Int. J. Struct. Stabil. Dynam. 22 (5), 2250053. http://doi.org/10.1142/s0219455422500535.
Dai, K., Fang, C., Zhang, S., Shi, Y., 2021. Conceptual design and numerical study on a cable-based energy dissipating system for the vibration reduction of tower-like structures. Eng. Struct. 237, 112034. http://doi.org/10.1016/j.engstruct.2021.112034.
Datta, T.K., 2010. Seismic Analysis of Structures. John Wiley & Sons (Asia) Pte. Ltd., Singapore. http://doi.org/10.1002/9780470824634.
Den Hartog, J.P., 1947. Mechanical Vibrations. McGraw-Hill Book Company Inc, USA.
Ding, H., Altay, O., Wang, J.-T., 2023. Lateral vibration control of monopile supported offshore wind turbines with toroidal tuned liquid column dampers. Eng. Struct. 286, 116107. http://doi.org/10.1016/j.engstruct.2023.116107.
Fitzgerald, B., Sarkar, S., Staino, A., 2018. Improved reliability of wind turbine towers with active tuned mass dampers (ATMDs). J. Sound Vib. 419, 103–122. http://doi.org/10.1016/J.JSV.2017.12.026.
Ghassempour, M., Failla, G., Arena, F., 2019. Vibration mitigation in offshore wind turbines via tuned mass damper. Eng. Struct. 183, 610–636. http://doi.org/10.1016/j.engstruct.2018.12.092.
GWEC, 2022. Global Wind Report2022. Global Wind Energy Council, UK.
Hemmati, A., Oterkus, E., 2018. Semi-active structural control of offshore wind turbines considering damage development. J. Mar. Sci. Eng. 6, 102. https://doi.org/10.3390/jmse6030102.
Hu, Y., Chen, M.Z., Li, C., 2017. Active structural control for load mitigation of wind turbines via adaptive sliding-mode approach. J. Franklin Inst. 354, 4311–4330. http://doi.org/10.1016/j.jfranklin.2017.04.002.
Huang, X., Liu, X., Sun, J., Zhang, Z., Hua, H., 2014. Vibration isolation characteristics of a nonlinear isolator using Euler buckled beam as negative stiffness corrector: a theoretical and experimental study. J. Sound Vib. 333, 1132–1148. https://doi.org/10.1016/j.jsv.2013.10.026.
Hussan, M., Rahman, M.S., Sharmin, F., Kim, D., Do, J., 2018. Multiple tuned mass damper for multi-mode vibration reduction of offshore wind turbine under seismic excitation. Ocean Eng. 160, 449–460. https://doi.org/10.1016/j.oceaneng.2018.04.041.
Ikago, K., Saito, K., Inoue, N., 2012. Seismic control of single-degree-of-freedom structure using tuned viscous mass damper. Earthq. Eng. Struct. Dynam. 41 (3), 453–474. https://doi.org/10.1002/eqe.1138.
Jahangiri, V., Sun, C., Kong, F., 2021. Study on a 3D pounding pendulum TMD for mitigating bi-directional vibration of offshore wind turbines. Eng. Struct. 241, 112383. https://doi.org/10.1016/j.engstruct.2021.112383.
Jonkman, J., Butterfield, S., Musial, W., Scott, G., 2009. Definition of A 5-MW Reference Wind Turbine for Offshore System Development. National Renewable Energy Laboratory, Golden, CO, USA. https://doi.org/10.2172/947422.
Kampitsis, A., Kapasakalis, K., Via-Estrem, L., 2022. An integrated FEA-CFD simulation of offshore wind turbines with vibration control systems. Eng. Struct. 254, 113859. https://doi.org/10.1016/j.engstruct.2022.113859.
Kapasakalis, K.A., Antoniadis, I.A., Sapountzakis, E.J., 2020. Performance assessment of the KDamper as a seismic absorption base. Struct. Control Health Monit. 27 (4), e2482. https://doi.org/10.1002/stc.2482.
Kapasakalis, K.A., Antoniadis, I.A., Sapountzakis, E.J., 2021. Constrained optimal design of seismic base absorbers based on an extended KDamper concept. Eng. Struct. 226, 111312. https://doi.org/10.1016/j.engstruct.2020.111312.
Kapasakalis, K., Mantakas, A., Kalderon, M., Antoniou, M., Sapountzakis, E., 2023. Performance evaluation of distributed extended kdamper devices for seismic protection of mid-rise building structures. J. Earthq. Eng. https://doi.org/10.1080/13632469.2023.2226227.
Le, T.D., Ahn, K.K., 2011. A vibration isolation system in low frequency excitation region using negative stiffness structure for vehicle seat. J. Sound Vib. 330, 6311–6335. http://doi.org/10.1016/j.jsv.2011.07.039.
Le, T.D., Ahn, K.K., 2012. Fuzzy sliding mode controller of a pneumatic active isolating system using negative stiffness structure. J. Mech. Sci. Technol. 26, 3873–3884. http://doi.org/10.1007/s12555-014-0150-0.
Le, T.D., Ahn, K.K., 2013. Experimental investigation of a vibration isolation system using negative stiffness structure. Int. J. Mech. Sci. 70, 99–112. http://doi.org/10.1016/J.IJMECSCI.2013.02.009.
Leng, D., Wang, R., Yang, Y., Li, Y., Liu, G., 2023. Study on a three-dimensional variable-stiffness TMD for mitigating bi-directional vibration of monopile offshore wind turbines. Ocean Eng. 281, 114791. https://doi.org/10.1016/j.oceaneng.2023.114791.
Li, H., Li, Y., Li, J., 2020. Negative stiffness devices for vibration isolation applications: a review. Adv. Struct. Eng. 23 (8), 1739–1755. https://doi.org/10.1177/1369433219900311.
Lin, G.-L., Lu, L.-Y., Lei, K.-T., Liu, K.-Y., Ko, Y.-Y., Ju, S.-H., 2021. Experimental study on seismic vibration control of an offshore wind turbine with TMD considering soil liquefaction effect. Mar. Struct. 77, 102961. https://doi.org/10.1016/j.marstruc.2021.102961.
Liu, G., Lei, Z., Wang, H., 2021. Investigation and optimization of a pre-stressed tuned mass damper for wind turbine tower. Struct. Control Health Monit. 29 (3), e2894. https://doi.org/10.1002/stc.2894.
Liu, W., Ikago, K., 2021. Experimental study of earthquake input energy of low-frequency structures equipped with a passive rate-independent damping device. Struct. Control Health Monit. 29 (2), 2883. https://doi.org/10.1002/stc.2883.
Liu, W., Ikago, K., 2022a. Causal implementation of rate-independent linear damping for the seismic protection of low-frequency structures. Structures 35, 274–288. https://doi.org/10.1016/j.istruc.2021.10.095.
Liu, W., Ikago, K., 2022b. Performance of a passive rate-independent damping device in a seismically isolated multistory building. Struct. Control Health Monit. 29, e2941. https://doi.org/10.1002/stc.2941.
Liu, W., Ikago, K., 2022c. Feasibility of physical implementation of rate-independent linear damping to protect multistory low-frequency structures. J. Sound Vib. 528, 116893. https://doi.org/10.1016/j.jsv.2022.116893.
Liu, W., Ikago, K., Wu, Z., Fukuda, I., 2022a. Modified tuned Maxwell-Wiechert model for improving seismic performance of base-isolated structures. J. Build. Eng. 54, 104616. https://doi.org/10.1016/j.jobe.2022.104616.
Liu, W., Liu, J., 2023. Experimental realization of rate-independent linear damping using a semiactive damper to enhance the seismic performance of low-frequency structures. J. Build. Eng. 70, 106374. https://doi.org/10.1016/j.jobe.2023.106374.
Liu, W., Ni, Y.Q., Ikago, K., Ao, W.K., 2023. Seismic control of base-isolated structures using rate-independent damping devices. J. Build. Eng. 78, 107744. https://doi.org/10.1016/j.jobe.2023.107744.
Liu, X., Huang, X., Hua, H., 2013. On the characteristics of a quasi-zero stiffness isolator using Euler buckled beam as negative stiffness corrector. J. Sound Vib. 332 (14), 3359–3376. https://doi.org/10.1016/j.jsv.2012.10.037.
Liu, X., Xu, J., He, G., Chen, C., 2022b. Lateral vibration mitigation of monopile offshore wind turbines with a spring pendulum pounding tuned mass damper. Ocean. Eng. 266, 112954. https://doi.org/10.1016/j.oceaneng.2022.112954.
Liu, Z., Wang, Y., Hua, X., Zhu, H., Zhu, Z., 2020. Optimization of wind turbine TMD under real wind distribution countering wake effects using GPU acceleration and machine learning technologies. J. Wind Eng. Ind. Aerod. 28, 104436. https://doi.org/10.1016/j.jweia.2020.104436.
Molyneux, W., 1957. Supports for Vibration Isolation. Her Majesty's Stationery Office, UK.
Niu, F., Meng, L., Wu, W., Sun, J., Zhang, W., Meng, G., Rao, Z., 2014. Design and analysis of a quasi-zero stiffness isolator using a slotted conical disk spring as negative stiffness structure. J. Vibroeng. 16, 1769–1785.
Pasala, D., Sarlis, A., Nagarajaiah, S., Reinhorn, A., Constantinou, M., Taylor, D., 2013. Adaptive negative stiffness: new structural modification approach for seismic protection. J. Struct. Eng. 139, 1112–1123. https://doi.org/10.1061/(ASCE)ST.1943-541X.0000615.
Rahman, M., Ong, Z.C., Chong, W.T., Julai, S., Khoo, S.Y., 2015. Performance enhancement of wind turbine systems with vibration control: a review. Renew. Sustain. Energy Rev. 51, 43–54. https://doi.org/10.1016/j.rser.2015.05.078.
Sapountzakis, E., Syrimi, P., Pantazis, I., Antoniadis, I., 2017. KDamper concept in seismic isolation of bridges with flexible piers. Eng. Struct. 153, 525–539. https://doi.org/10.1016/j.engstruct.2017.10.044.
Sarkar, S., Chakraborty, A., 2018. Optimal design of semiactive MR-TLCD for along-wind vibration control of horizontal axis wind turbine tower. Struct. Control Health Monit. 25 (2), e2083. https://doi.org/10.1002/stc.2083.
Shi, X., Zhu, S., 2015. Magnetic negative stiffness dampers. Smart Mater. Struct. 24, 072002. http://doi.org/10.1088/0964-1726/24/7/072002.
Smith, M.C., 2002. Synthesis of mechanical networks: the inerter. IEEE Trans. Automat. Control 47 (10), 1648–1662. http://doi.org/10.1109/TAC.2002.803532.
Soltani, P., Deraemaeker, A., 2022. Pendulum tuned mass dampers and tuned mass dampers: analogy and optimum parameters for various combinations of response and excitation parameters. J. Vib. Control 28, 2004–2019. https://doi.org/10.1177/10775463211003414.
Sun, C., 2018. Semi-active control of monopile offshore wind turbines under multi-hazards. Mech. Syst. Signal Process. 99, 285–305. https://doi.org/10.1016/j.ymssp.2017.06.016.
Wang, M., Zhang, W.-Q., Wang, P.-G., Du, X.-L., 2023. Multiple hazards vibration control of jacket offshore wind turbines equipped with amplifying damping transfer systems: winds, waves, and earthquakes. Ocean Eng. 285, 115355. https://doi.org/10.1016/j.oceaneng.2023.115355.
Wang, P., Xu, Y., Zhang, X., Xi, R., Du, X., 2021. A substructure method for seismic responses of offshore wind turbine considering nonlinear pile-soil dynamic interaction. Soil Dynam. Earthq. Eng. 144, 106684. https://doi.org/10.1016/j.soildyn.2021.106684.
Wang, W., Li, X., Zhao, H., Wang, B., Li, Y., 2020. Vibration control of a pentapod offshore wind turbine under combined seismic wind and wave loads using multiple tuned mass damper. Appl. Ocean Res. 103, 102254. https://doi.org/10.1016/j.apor.2020.102254.
Xu, D., Yu, Q., Zhou, J., Bishop, S., 2013. Theoretical and experimental analyses of a nonlinear magnetic vibration isolator with quasi-zero-stiffness characteristic. J. Sound Vib. 332, 3377–3389. http://doi.org/10.1016/j.jsv.2013.01.034.
Zhang, J., Yuan, G.-K., Zhu, S., Gu, Q., Ke, S., Lin, J., 2022. Seismic analysis of 10 MW offshore wind turbine with large-diameter monopile in consideration of seabed liquefaction. Energies 15 (7), 2539. https://doi.org/10.3390/en15072539.

Zhang, R., Zhao, Z., Dai, K., 2019a. Seismic response mitigation of a wind turbine tower using a tuned parallel inerter mass system. Eng. Struct. 180, 29–39. https://doi.org/10.1016/j.engstruct.2018.11.020.

Zhang, T., Wang, W., Li, X., Wang, B., 2023. Vibration mitigation in offshore wind turbine under combined wind-wave-earthquake loads using the tuned mass damper inerter. Renew. Energ. 216, 119050. https://doi.org/10.1016/j.renene.2023.119050.

Zhang, Z., Basu, B., Nielsen, S.R., 2019b. Real-time hybrid aeroelastic simulation of wind turbines with various types of full-scale tuned liquid dampers. Wind Energy 22, 239–256. https://doi.org/10.1002/we.2281.

Zhao, B., Gao, H., Wang, Z., Lu, Z., 2018. Shaking table test on vibration control effects of a monopile offshore wind turbine with a tuned mass damper. Wind Energy 21 (12), 1309–1328. https://doi.org/10.1002/we.2256.

Zuo, H., Bi, K., Hao, H., 2020. Simultaneous out-of-plane and in-plane vibration mitigations of offshore monopile wind turbines by tuned mass dampers. Smart Struct. Syst. 26 (4), 435–449. https://doi.org/10.12989/sss.2020.26.4.435.

Zuo, H., Zhang, J., Yuan, G.K., Zhu, S., 2022. Wind-and sea wave-induced response mitigations of offshore wind turbines using track nonlinear energy sinks. Struct. Control Health Monit. 29 (9), e2990. https://doi.org/10.1002/stc.2990.

Zuo, H., Zhu, S., 2022. Development of novel track nonlinear energy sinks for seismic performance improvement of offshore wind turbine towers. Mech. Syst. Signal Process. 172, 108975. https://doi.org/10.1016/j.ymssp.2022.108975.